JOURNAL OF PETROLOGY | VOLUME 54 | NUMBER 4 | PAGES 665–701 | 2013 | doi:10.1093/petrology/egs081

The Processes of Melt Differentiation in Arc Volcanic Rocks: Insights from OIB-type Arc Magmas in the Central Mexican Volcanic Belt

SUSANNE M. STRAUB[1]*, ARTURO GÓMEZ-TUENA[2], GEORG F. ZELLMER[3], RAMON ESPINASA-PERENA[4], FINLAY M. STUART[5], YUE CAI[1,6], CHARLES H. LANGMUIR[7], ANA LILLIAN MARTIN-DEL POZZO[8] AND GARY T. MESKO[1]

[1]LAMONT–DOHERTY EARTH OBSERVATORY AT THE COLUMBIA UNIVERSITY, 61 ROUTE 9W, PALISADES, NY 10964, USA

[2]CENTRO DE GEOCIENCIAS, UNIVERSIDAD NACIONAL AUTÓNOMA DE MÉXICO, QUERÉTARO 76230, MEXICO

[3]INSTITUTE OF EARTH SCIENCES, ACADEMIA SINICA, 128 ACADEMIA ROAD, SEC. 2, NANKANG, TAIPEI 11529, TAIWAN

[4]CENTRO NACIONAL DE PREVENCIÓN DE DESASTRES, SECRETARÍA DE GOBERNACIÓN, AV. DELFÍN MADRIGAL 665, COL. PEDREGAL DE SANTO DOMINGO C.P. 04360, DELEGACIÓN COYOACÁN, MÉXICO D.F., MEXICO

[5]ISOTOPE GEOSCIENCES UNIT, SCOTTISH UNIVERSITIES RESEARCH AND REACTOR CENTRE, EAST KILBRIDE G75 0QF, UK

[6]DEPARTMENT OF EARTH AND ENVIRONMENTAL SCIENCES, COLUMBIA UNIVERSITY, 61 ROUTE 9W, PALISADES, NY 10964, USA

[7]DEPARTMENT OF EARTH AND PLANETARY SCIENCES, HARVARD UNIVERSITY, 20 OXFORD STREET, CAMBRIDGE, MA 02137, USA

[8]INSTITUTO DE GEOFISICA, UNIVERSIDAD NACIONAL AUTÓNOMA DE MÉXICO, CIUDAD UNIVERSITARIA, MEXICO, D.F. 04510, MEXICO

RECEIVED FEBRUARY 16, 2012; ACCEPTED OCTOBER 19, 2012
ADVANCE ACCESS PUBLICATION NOVEMBER 29, 2012

Andesite petrogenesis is inextricably linked to plate processing at convergent margins. The details of andesite formation, however, remain poorly understood because the signatures of the initial arc mantle melts are often modified in the overlying crust. To distinguish initial mantle from crustal signatures in arc magmas, we studied two compositionally zoned Holocene monogenetic volcanoes, Texcal Flow and Volcan Chichinautzin, in the central Mexican Volcanic Belt (MVB). Texcal Flow and V. Chichinautzin erupt 'ocean island basalt (OIB)-type', high-Nb (17–36 ppm), olivine-phyric basalts to basaltic andesites (49·4–57·3 wt % SiO_2; Mg# = 68–50) that show an arc affinity in their major element oxides. At both volcanoes melt SiO_2 increases with time. However, systematic changes of melt SiO_2 with $^{87}Sr/^{86}Sr$ and $^{143}Nd/^{144}Nd$, the overall low $^{87}Sr/^{86}Sr = 0{\cdot}70305–0{\cdot}70453$ and high $^{143}Nd/^{144}Nd = 0{\cdot}51273–0{\cdot}51299$ relative to continental crust, and the high $^{3}He/^{4}He = 7–8$ R_a of olivine phenocrysts preclude melt silica enrichment by crustal assimilation and fractional crystallization. Instead, the data require the existence of silicic initial mantle melts. The high Ni abundances of olivines suggest that the silicic melts originate from segregations of 'reaction pyroxenites' that formed in the peridotite mantle wedge following multiple infiltrations of silicic slab components. Sequential melting of zoned silica-deficient to silica-excess pyroxenites can reproduce the time-progressive evolution of melt silica content at Texcal Flow and V. Chichinautzin. As initial melts always have high Mg# > 70 regardless of their SiO_2 content, the low-Mg# values of the magmas erupted must reflect loss of moderate amounts

*Corresponding author. Telephone: +845 365 8464. Fax: +845 365 8155. E-mail: smstraub@ldeo.columbia.edu

(<15%) of olivine and possibly pyroxenes at crustal levels. Fractional crystallization and recharge mixing nearly erase all mantle signatures in the most silicic V. Chichinautzin magmas, so that their origin can only be inferred from their association with the more mafic precursory melts. The pyroxenite model implies that ~15–18 wt % of the erupted melt mass, and possibly more, is slab-derived. We infer that the elements Fe, Mg, Ca and Ti are principally mantle-derived, whereas significant amounts of the elements Si, K, Na, P and possibly Al may be contributed from slab. As blends of mantle and slab materials, the OIB-type Texcal Flow and V. Chichinautzin magmas provide limited indication of the composition of the sub-arc mantle prior to subduction modification, which is inferred to be similar to primitive mantle, but less enriched than the sources of the intraplate magmas behind the MVB volcanic front.

KEY WORDS: *arc magma genesis; melt differentiation; major elements; Mexican Volcanic Belt*

INTRODUCTION

The major element composition of andesitic magmas in subduction zones is distinct from that of magmas erupted at mid-ocean ridges and intraplate volcanoes (e.g. Gill, 1981; Tatsumi & Eggins, 1995). Because major element oxides make up >99% of the melt mass, understanding the causes of this difference is essential for calculating the chemical fluxes associated with arc magmatism (e.g. Plank & Langmuir, 1993; Straub *et al.*, 2011*a*). However, the petrogenesis of arc andesites remains contested. One group of models proposes that basaltic melts are generated in the sub-arc mantle, and that andesites form subsequently in the overlying crust by fractional crystallization and assimilation of silicic crustal material (e.g. Eichelberger, 1978; Gill, 1981; Leeman, 1983; Hildreth & Moorbath, 1988; Plank & Langmuir, 1988; Tamura & Tatsumi, 2002; Annen *et al.*, 2006; Streck *et al.*, 2007; Reubi & Blundy, 2009). Other models favor the formation of initial silicic arc melts beneath the Moho, for which various mechanisms have been proposed. These range from slab melting (Kay, 1978; Defant & Drummond, 1990), to hydrous melting of peridotite (Baker *et al.*, 1994; Hirose, 1997; Blatter & Carmichael, 1998*b*; Moore & Carmichael, 1998; Carmichael, 2002), to hybridization of slab and mantle materials by melt rock reaction processes (Yogodzinksi *et al.*, 1994, 1995; Kelemen, 1995; Rapp *et al.*, 1999; Kelemen *et al.*, 2003, 2004; Gómez-Tuena *et al.*, 2007a; Straub *et al.*, 2011*a*). Of course, these various models could apply to different degrees in different arcs, and even within a single arc, depending on the subduction parameters.

The key to distinguishing among these petrogenetic models of melt generation lies in unraveling the processes of differentiation that affect arc magmas between their formation and eruption. This is a difficult task, as crustal differentiation is a complex and multi-stage process (e.g. Leeman, 1983; Hildreth & Moorbath, 1988; Plank & Langmuir, 1988; Reubi & Blundy, 2009; Kent *et al.*, 2010). Moreover, it has become increasingly clear that even arc magmas erupted in close temporal and spatial proximity can have different genetic roots (e.g. Wallace & Carmichael, 1999; Schaaf *et al.*, 2005). A particularly promising approach to understanding the processes of melt differentiation is the investigation of a magma series from a single volcano–magma system that was erupted during a single volcanic episode. Such series are probably genetically linked, and least affected by the diverse processes of melt differentiation. This approach has widely been used for understanding the formation of high-silica magmas by means of studies of compositionally zoned ignimbrites (e.g. Robin *et al.*, 1994; Freundt & Schmincke, 1995). However, ignimbrites are rarely basaltic. Monogenetic volcanoes provide the opportunity to take such an approach for mafic magma systems (e.g. Reiners, 2002), particularly in the Mexican Volcanic Belt where mafic monogenetic volcanoes are unusually abundant in comparison with other arcs (Luhr & Carmichael, 1985; McBirney *et al.*, 1987; Marquez *et al.*, 1999; Blatter *et al.*, 2001; Siebe *et al.*, 2004*a*).

We present the results of a detailed chemical study of two zoned Holocene monogenetic volcanoes (Texcal Flow and V. Chichinautzin) that erupted within ~1100 years and ~6 km of each other in the central Mexican Volcanic Belt (MVB) (Fig. 1). Texcal Flow and V. Chichinautzin erupt basaltic and basaltic andesitic magmas, respectively, with an overall silica range from 49·4 to 57·3 wt % (Fig. 2; Siebe *et al.*, 2004*a*, 2004*b*; this study). The eruptive sequence can be reconstructed for each volcano and documents the compositional evolution of the magmas (Siebe *et al.*, 2004*a*, 2004*b*; this study). Although the chemistry of the Texcal Flow and V. Chichinautzin magmas has been studied previously (Wallace & Carmichael, 1999; Siebe *et al.*, 2004*a*; Straub *et al.*, 2008, 2011*a*), we have expanded this work by fully characterizing each of the eruptive units based on bulk-rock major elements, trace elements, $^{87}Sr/^{86}Sr$ and $^{143}Nd/^{144}Nd$, and previously published data on olivine compositions (Straub *et al.*, 2008, 2011*a*). The simple field relationships and the comprehensive chemical characterization allow us to unravel the causes of major element diversity of magmas erupted through the continental crust of the central MVB.

GEOLOGICAL BACKGROUND

Central Mexican Volcanic Belt

The geological setting of the Mexican Volcanic Belt (MVB) has been described in detail elsewhere (e.g. Gómez-Tuena *et al.*, 2007b; Ferrari *et al.*, 2011). Here, only a short summary pertinent to this study is given. The MVB is an active Pliocene–Quaternary volcanic arc related to the subduction of the Cocos and Rivera plates

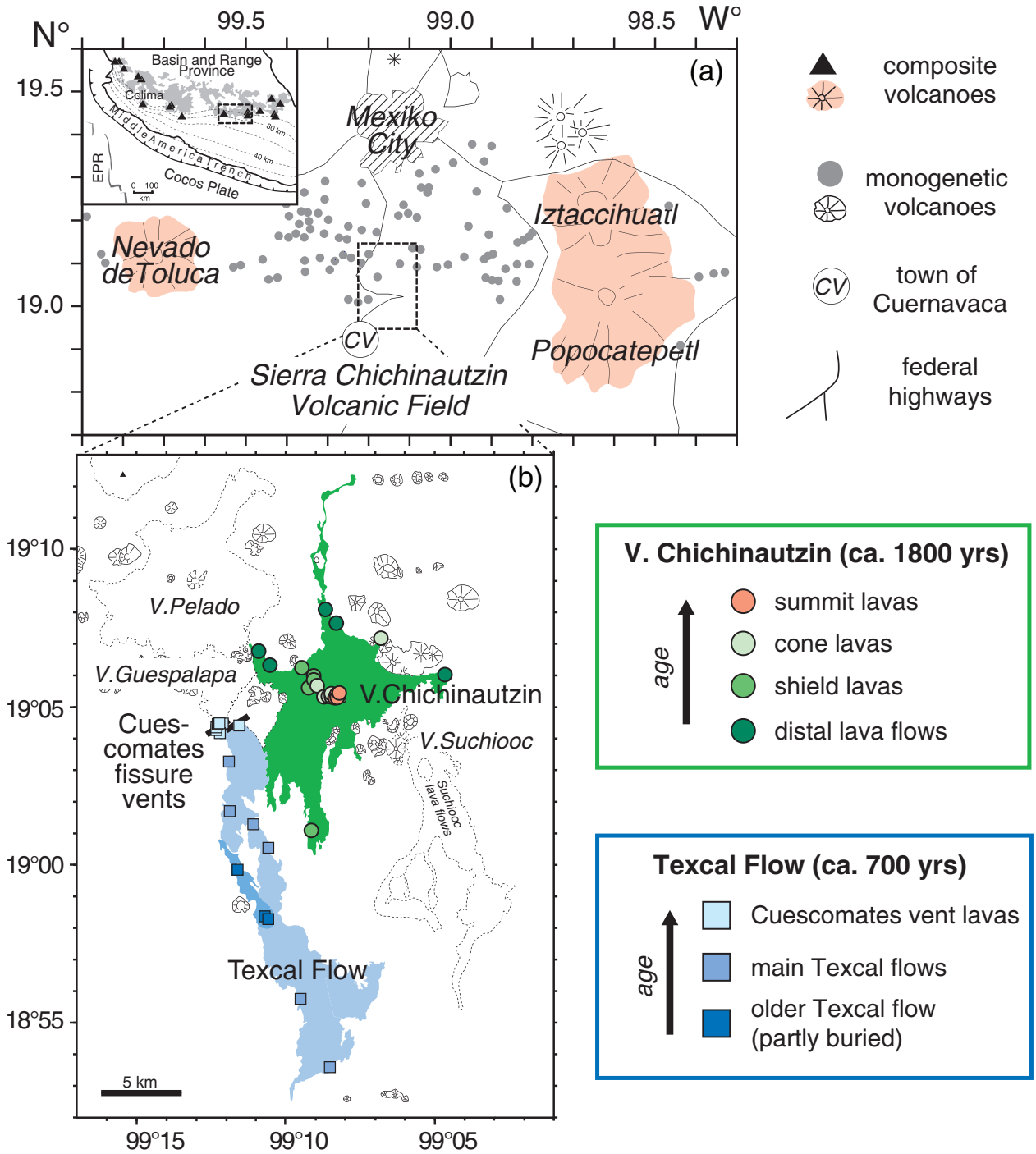

Fig. 1. Maps of the central Mexican Volcanic Belt. (a) Monogenetic volcanoes of the Sierra Chichinautzin Volcanic Field (SCVF) flanked by the Quaternary composite volcanoes Nevado de Toluca and Popocatepetl. Slab contours in inset after Pardo & Suarez (1995). (b) Enlargement of the central SCVF showing the Texcal Flow and V. Chichinautzin. Map, volcanic stratigraphy and volcano ages from Siebe *et al.* (2004*a*, 2004*b*) and this study.

along the Middle America Trench (Fig. 1). Crustal thickness reaches ~45 km in the central section between the composite volcanoes Popocatepetl and Nevado de Toluca (100–98°30'W; Perez-Campos *et al.*, 2008; Kim *et al.*, 2010) where the arc is constructed on a sialic crust of Proterozoic granulites and Mesozoic metapelites, granites and limestones (Gómez-Tuena *et al.*, 2007; Ortega-Gutiérrez *et al.*, 2008). The Middle America trench runs

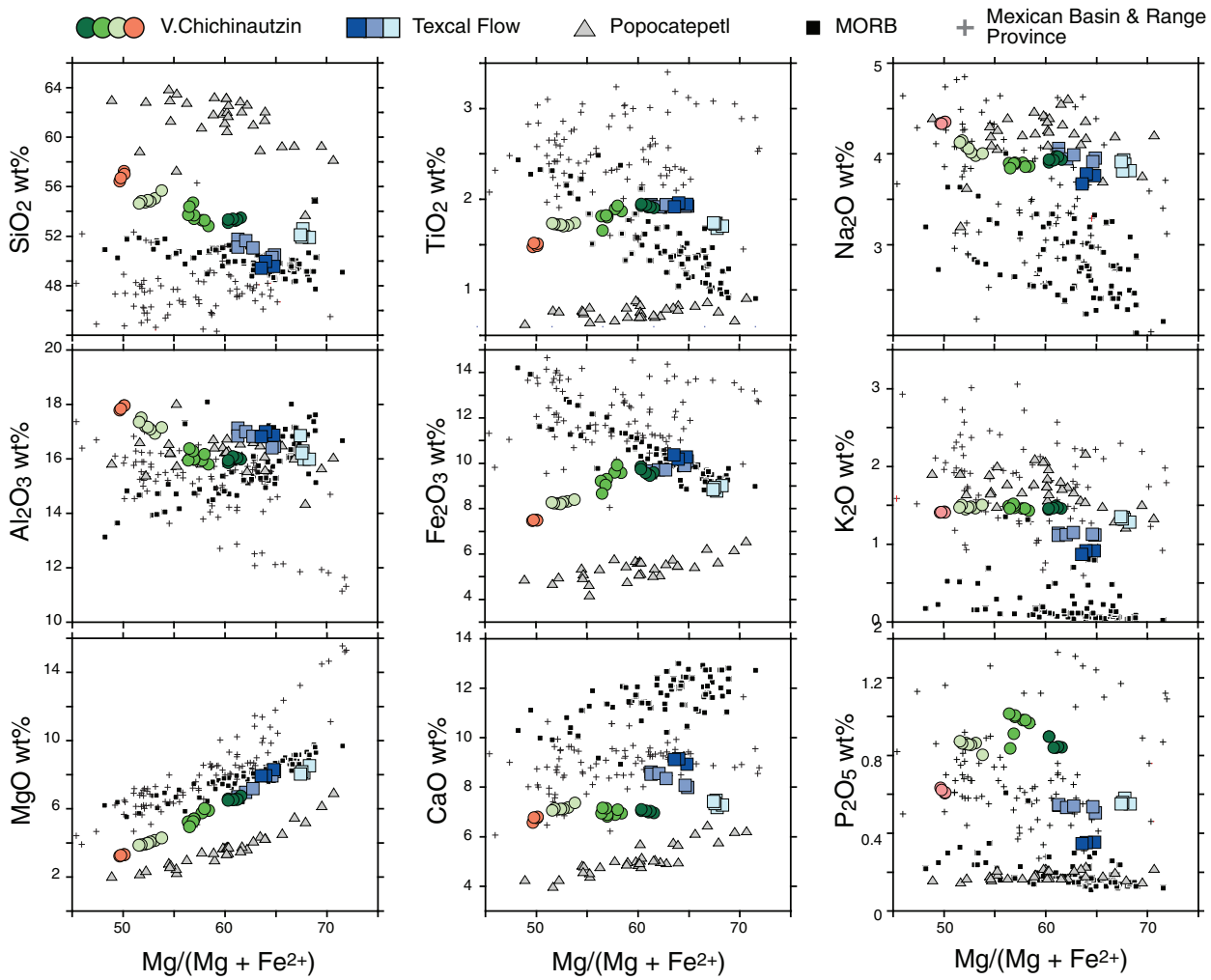

Fig. 2. Major element oxides (in wt %) vs bulk-rock Mg# number [= molar ratio of [Mg/(Mg + Fe^{2+})], calculated using 18% ferric iron after Straub *et al.* (2008)]. Also plotted are mid-ocean ridge basalts (MORB) from the East Pacific Rise (Niu & Batiza, 1997), basalts from the Mexican Basin and Range Province (Luhr *et al.*, 1989, 1995*a*, 1995*b*; Gómez-Tuena *et al.*, 2003) and Popocateptl volcanic rocks (Schaaf *et al.*, 2005).

obliquely at an angle of ~17° to the MVB, in response to the horizontal subduction of the slab between ~100 and 250 km from the trench (Fig. 1). In the central MVB, at ~280 km from the trench, the slab steepens abruptly to dip 65–75° beneath the arc front. Texcal Flow and V. Chichinautzin are located ~90 km above the slab at the volcanic arc front (Perez-Campos *et al.*, 2008; Kim *et al.*, 2010).

The central MVB erupts basaltic to dacitic magmas that include calc-alkaline magmas as well as 'ocean island basalt (OIB)-type' arc magmas, also referred to as 'high-Nb arc magmas', or 'high-Nb arc basalts' (HNAB). (e.g. Verma, 1999; Wallace & Carmichael, 1999; LaGatta, 2003; Schaaf *et al.*, 2005). The dominant calc-alkaline series display strong enrichment of large ion lithophile elements (LILE) relative to rare earth elements (REE) and high field strength elements (HFSE). This forms one end-member in compositional space, with the other end-member being the far less abundant OIB-type arc magmas. These are mildly alkaline basalts to basaltic andesites with high Nb = 16–35 ppm and Nb/La ~1 and enriched trace element patterns similar to those of intraplate magmas (Verma, 1999; Wallace & Carmichael, 1999; Schaaf *et al.*, 2005). OIB-type arc magmas cannot be derived from the continental crust and hence testify that mantle melts may ascend through the thick continental basement nearly unchanged (Wallace & Carmichael, 1999). OIB-type MVB magmas are often considered to best represent melts of the unmetasomatized Mexican subarc mantle. However, incipient relative depletions of Nb and Ta and enrichments of fluid-mobile LILE that develop with increasing melt SiO_2 content indicate the influence of a crustal component, which may be derived from either the subducted slab or the continental basement (Wallace & Carmichael, 1999; Gómez-Tuena *et al.*, 2003,

2007a, 2011; Schaaf *et al.*, 2005; Straub *et al.*, 2008). Thus, the OIB-type arc volcanoes Texcal Flow and V. Chichinautzin provide an exceptional perspective on the cause of major element diversity in arc-related volcanic rocks.

SITE SELECTION AND SAMPLING

Texcal Flow and V. Chichinautzin are monogenetic volcanoes of the Holocene Sierra Chichinautzin Volcanic Field (SCVF) in central Mexico (Fig. 1) that erupted within 6 km of each other. They belong to a cluster of OIB-type volcanoes that includes the volcanoes Xitle, La Cima, Yololica and Cajete. These volcanoes erupt olivine-phyric, mildly Na-alkaline arc basalts and basaltic andesites (Wallace & Carmichael, 1999; Siebe *et al.*, 2004*a*; Straub *et al.*, 2008) approximately halfway between the calc-alkaline composite volcanoes Popocatepetl and Nevado de Toluca (Wallace & Carmichael, 1999). Siebe *et al.* (2004*a*, 2004*b*) published the first geological maps of Texcal Flow and V. Chichinautzin, which were further refined in the present study (Fig. 1). Sampling took place during five annual field campaigns between January 2004 and January 2009. Each campaign was followed by bulk-rock analyses for major and trace elements, which were then used to direct sampling in the following year. This strategy ensured recognition and characterization of three and four successive erupted units at Texcal Flow and V. Chichinautzin, respectively, by means of stratigraphic position and rock chemistry. Petrographic differences between the eruptive units are subtle and secure identification of an eruptive unit requires chemical analysis. The volcanic rocks are typically dark to medium gray, dense to vesicular, and have phenocrysts of olivine with inclusions of Cr-spinel (see also Siebe *et al.*, 2004*a*). The size and volume percentage of olivine phenocrysts varies. In general, olivines tend to be largest (~1 mm) and most abundant (up to 7 vol. %) in MgO-rich samples, and gradually decrease with increasing melt silica content to sizes <0·5 mm and abundances <1 vol. % in silicic basaltic andesites (Siebe *et al.*, 2004*a*; this study). Plagioclase phenocrysts appear only in some of the most silicic samples. Siebe *et al.* (2004*a*) reported also some clino- and orthopyroxene microphenocrysts.

Texcal Flow

Siebe et al. (2004*a*, 2004*b*) viewed the Texcal Flow basalts as part of the Guespalapa Volcanic Complex, which formed between 2800 and 4700 BP. Our data show, however, that the Texcal Flow originates from two younger volcanic fissure vents (western and eastern 'Cuescomates vents') that breached the SW flank of the calc-alkaline Guespalapa shield at ~700 BP [age data from Siebe *et al.*, 2004*b*] (Fig. 1). The Nb-rich (17–26 ppm Nb) Texcal Flow basalts are clearly different from the basaltic andesitic and andesitic lavas of the Guespalapa shield, which have low Nb (~4–9 ppm), despite similar enrichment levels of the LILE (Siebe *et al.*, 2004*a*; Straub *et al.*, 2011*b*). The Texcal lavas flow downhill to the south over a length of 24 km onto the plain of Cuernavaca (Siebe *et al.*, 2004*b*). The thickness and hence the erupted volume of the Texcal Flow are unknown, but the erupted volume is thought to be similar to that of V. Chichinautzin (Siebe *et al.*, 2004*b*). Stratigraphy and bulk-rock compositions indicate three different, successively erupted magma batches. The oldest Texcal lavas ('old Texcal flow', three samples) belong to an olivine-phyric flow that is mostly buried beneath the later flows. The second stage ('main Texcal flow', five samples) produced far more voluminous flows, which are petrographically indistinguishable from the old Texcal flow and make up the bulk of the Texcal Flow outside the Cuescomates vent area. Subtle chemical differences suggest additional zoning within the main Texcal Flow, but these were not pursued further. The Cuescomates vent lavas ('vent lavas', seven samples) erupted in the waning stage. The vent lavas are either plagioclase–olivine-phyric, or aphyric, but do not show any significant difference in chemistry, including MgO and Ni, which are sensitive to olivine loss from the melt. The vent magmas are either emplaced as lava flows in proximity to the fissure vents or form spatter cones several meters high.

Volcan Chichinautzin

With an eruptive volume of at least ~0·55–1·1 km^3 and an eruptive age of 183 BP, V. Chichinautzin is one of the youngest and largest monogenetic volcanoes of the SCFV (Siebe *et al.*, 2004*b*). The basaltic andesites of V. Chichinautzin form a shallow shield on which a younger cone has been constructed (Siebe *et al.*, 2004*a*, 2004*b*). Based on stratigraphy, petrography and composition, four eruptive units have been distinguished (Fig. 1). The oldest group ('distal lava flows', six samples) consists of lava flows that extend up to 9 km northward and up to 4 km eastward from the base of the Chichinautzin shield (Siebe *et al.*, 2004*a*, 2004*b*). The distal lava flows are olivine-phyric and form thin (~0·5–1 m) flow units of pahoehoe-like appearance. The second group ('shield lavas', seven samples) forms the gently sloping basal shield between ~3120 and ~3190 m above sea level. Southwards, the shield lavas flow downhill towards the city of Cuernavaca. The petrography of the shield lavas is very similar to that of the older flows, with abundant quartz–pyroxene glomerocrysts. The third group ('cone lavas', seven samples) builds the younger cone with steeper flanks on top of the shield, and includes the prominent western rim of V. Chichinautzin. The cone lavas are olivine–plagioclase-phyric, more viscous lavas that resemble aa flows. The fourth group ('summit lavas', four samples) is volumetrically by far the smallest group. It comprises the youngest lavas, which constructed a small cone on the eastern rim and fill the summit bowl, and may spill onto the slopes of the upper cone in the east and

west. The summit lavas also resemble aa flows, but unlike in the cone lavas, plagioclase dominates over olivine.

Samples and analytical methods

We obtained 13 samples from Texcal Flow and 24 samples from V. Chichinautzin (Table 1). Bulk-rock powders were analyzed by X-ray fluorescence (XRF) and direct current plasma emission spectroscopy methods for major elements (35 samples, excluding two samples from Texcal Flow) at the Geoanalytical Laboratory of Washington State University, USA and at the Department of Earth and Planetary Sciences (Langmuir Laboratory) at Harvard University, USA. Trace elements P, Sc, V, Ni, Cr, Co, Li, Be, Cs, Ba, U, Tl, Rb, Th, Nb, Ta, La, Ce, Pb, Pr, Sr, Nd, Sm, Hf, Zr, Eu, Gd, Tb, Dy, Y, Ho, Er, Yb and Lu for 37 samples were determined by inductively coupled plasma mass spectrometry (ICP-MS) methods at the Centro de Geociencias (CGEO, 25 samples), Universidad Nacional Autónoma de México, Querétaro, México and at the Department of Earth and Planetary Sciences (Langmuir Laboratory) at Harvard University, USA (14 samples). A subset (nine samples from Texcal Flow and 17 samples from V. Chichinautzin) was analyzed for Sr and Nd isotope ratios by thermal ionization mass spectrometry at the Institute for Earth Sciences (IES), Academia Sinica, Taipei, Taiwan (25 samples), and at the Lamont–Doherty Earth Observatory of Columbia University in Palisades, USA (five samples) (Table 1). Subsets of samples for major and trace elements and radiogenic isotopes were analyzed in either laboratory to preclude interlaboratory bias. Details can be found in the Supplementary Data together with details of sample preparation, analytical methods and standard information (available for downloading at http://www.petrology.oxfordjournals.org/).

Some of the whole-rock abundance data have been previously reported by Straub et al. (2011a) as indicated in Table 1. Straub et al. (2011a) also reported $^{3}He/^{4}He$ and most of the compositional data for Texcal and V. Chichinautzin olivines. Here, some additional electron microprobe data for olivine phenocrysts are presented (sample S8, V. Chichinautzin shield) as well as for inclusions of Cr-spinel in olivine (Electronic Appendix Table 1 and 2). However, in this study we discuss these data for the first time with respect to the evolution of single volcanoes.

RESULTS

Temporal trends in the bulk-rocks of Texcal Flow and V. Chichinautzin

Major element oxides

The major element oxide compositional variations are presented in Fig. 2. Texcal Flow eruptive rocks are basalts (49·4–52·6 wt % SiO_2; 6·7–8·5 wt % MgO) whereas those from V. Chichinautzin are basaltic andesites (52·8–57·2 wt % SiO_2; 3·2–6·8 wt % MgO). Together they form a fairly coherent series that ranges from high-Mg# ~68 magmas close to equilibrium with mantle melts to low-Mg# ~50 magmas that are comparable with the upper continental crust (Rudnick & Gao, 2002). As in other Mexican monogenetic volcanoes (Wilcox, 1954; Luhr & Carmichael, 1985; McBirney et al., 1987), and as reported previously (Siebe et al., 2004a), silica increases with time in both volcanoes. The high sample density, however, reveals for the first time that the trends are not continuous, but form 'clusters' defined by the eruptive units. The 'clustering' is not a sampling artifact, because the sample locations are well distributed over the volcanic edifices with no indication of transitional compositions near the boundaries of the stratigraphic units. It should be noted also that within some stratigraphic units of V. Chichinautzin single clusters of data for SiO_2 vs Mg# define trends at an angle to the overall trend of the data. Only at V. Chichinautzin does SiO_2 increase steadily with decreasing Mg# and Ni within the overall trend of the data. At Texcal Flow, SiO_2 first increases as Mg# and Ni decrease, but the youngest, partly aphyric Texcal magmas have the highest SiO_2, Mg# and Ni (light coloured squares in Fig. 2). Examination of other major elements shows additional complexity. The trends in CaO are not smooth, and the K_2O, P_2O_5 and TiO_2 trends are not consistent with a single liquid line of descent. These observations already indicate that the silicic low-Mg# magmas may not be derivative melts (i.e. magma derived by fractional crystallization) from a single high-Mg# parental magma composition.

Trace elements

The high-Mg# magmatic rocks of Texcal Flow and V. Chichinautzin have the high Ni = 200 ppm and Cr = 300 ppm typical of the central MVB. Incompatible trace elements normalized to primitive mantle of McDonough & Sun (1995) reveal no, or only incipient 'arc-type' trace element signatures (Fig. 3). [Note that strong relative enrichments of Pb and Cs appear when normalized to primitive mantle, or normal mid-ocean ridge basalt (N-MORB), of Sun & McDonough (1989)]. The arc-type signature increases with increasing melt SiO_2, as relative depletions of Nb, Ta and Ti develop together with incipient relative enrichments of Cs, Ba, U and Pb (Fig. 4). However, the emergence of the arc signature does not imply an increase of the abundance level. The abundance of most incompatible elements first increases with increasing melt SiO_2, but mostly peaks in the shield and cone lavas of V. Chichinautzin prior to decreasing in the most silicic summit lavas that have the strongest arc signature. A striking exception is Sr, which remains nearly constant in abundance despite the variation of the other LILE.

Relative to the pyrolite of McDonough & Sun (1995), La/Sm_n values (normalized to pyrolite) of the Texcal Flow

Table 1: Abundances of major and trace elements, and Sr and Nd isotope ratios of Texcal Flow and V. Chichinautzin

Stratigraphic unit	Sample no.	Laboratory[1]	Longitude (W)	Latitude (N)	SiO_2	TiO_2	Al_2O_3	Fe_2O_3	MnO	MgO	CaO	Na_2O	K_2O
V. Chichinautzin													
Distal flows	MCH-06-5	WSU/CGEO	99°04′40″	19°06′02″	53·49	1·90	15·99	9·60	0·16	6·75	6·97	3·94	1·46
Distal flows	CH-08-5	WSU/CGEO	99°04′38″	19°05′59″	53·25	1·91	16·06	9·52	0·16	6·56	7·00	3·98	1·49
Distal flows	MCH-06-4	WSU/CGEO	99°08′14″	19°07′47″	53·35	1·92	16·04	9·46	0·16	6·55	7·04	3·97	1·47
Distal flows	MCH-06-2	WSU/CGEO	99°10′27″	19°06′25″	53·09	1·93	15·85	9·85	0·16	6·58	7·05	3·91	1·44
Distal flows	MCH-06-3	WSU/CGEO	99°08′40″	19°08′06″	53·42	1·94	16·09	9·59	0·16	6·53	7·05	3·93	1·46
Distal flows	MCH-06-1	WSU/CGEO	99°10′50″	19°06′50″	53·34	1·95	15·94	9·74	0·16	6·50	7·10	3·94	1·46
Shield	ASC1__S	Harvard	99°09′08″	19°01′06″	52·83	1·87	15·81	9·58	0·16	5·91	6·95	3·86	1·43
Shield	ASC1__A	Harvard	99°09′08″	19°01′06″	53·30	1·89	15·95	9·60	0·16	5·76	6·90	3·90	1·46
Shield	ASC1[2]	LaGatta (2003)	99°09′08″	19°01′06″									
Shield	S11	Harvard	99°09′27″	19°06′17″	53·41	1·82	15·98	9·29	0·16	5·40	6·83	3·90	1·47
Shield	S9	Harvard	99°09′14″	19°05′37″	53·71	1·80	15·98	9·31	0·16	5·41	6·89	3·90	1·50
shield	S10	Harvard	99°09′14″	19°05′37″	53·74	1·81	15·95	9·23	0·16	5·24	6·95	3·90	1·49
Shield	MCH-06-7	WSU/CGEO	99°06′48″	19°07′10″	54·71	1·82	16·29	9·05	0·16	5·24	7·15	3·90	1·52
Shield	S8	Harvard	99°09′03″	19°05′52″	54·39	1·66	16·38	8·66	0·15	4·95	7·17	3·84	1·46
Cone	S3	Harvard	99°08′27″	19°05′20″	54·73	1·72	17·20	8·22	0·14	3·94	7·12	4·08	1·45
Cone	S7	Harvard	99°08′57″	19°05′41″	55·06	1·71	16·93	8·33	0·14	4·15	7·18	3·98	1·46
Cone	S6	Harvard	99°08′57″	19°05′41″	54·84	1·70	17·09	8·30	0·14	4·06	7·13	4·02	1·48
Cone	S2	Harvard	99°08′21″	19°05′18″	54·92	1·72	17·17	8·21	0·14	3·98	7·12	4·06	1·47
Cone	S4	Harvard	99°08′34″	19°05′21″	54·81	1·73	17·51	8·25	0·15	3·89	7·14	4·15	1·51
Cone	CH-07-18	WSU/CGEO	99°09′03″	19°05′57″	55·70	1·74	17·16	8·39	0·15	4·29	7·37	4·01	1·51
Cone	S5	Harvard	99°08′43″	19°05′20″	54·65	1·74	17·36	8·27	0·14	3·87	7·07	4·13	1·47
Summit	S1	Harvard	99°08′17″	19°05′18″	56·45	1·48	17·79	7·46	0·13	3·24	6·57	4·34	1·41
Summit	CH-07-16	WSU/CGEO	99°08′17″	19°05′25″	57·27	1·49	17·96	7·50	0·13	3·31	6·77	4·35	1·42
Dummit	CH-07-17	WSU/CGEO	99°08′28″	19°05′25″	57·01	1·51	17·96	7·49	0·13	3·31	6·81	4·35	1·41
Summit	CH-07-15	WSU/CGEO	99°08′12″	19°05′27″	56·70	1·52	17·85	7·50	0·13	3·27	6·78	4·33	1·41
Texcal Flow													
West Cuescomates	CH-05-16	WSU/CGEO	99°12′21″	19°04′23″	52·62	1·74	16·30	8·87	0·14	8·13	7·49	3·94	1·35
West Cuescomates	S12B	Harvard	99°12′21″	19°04′18″	51·98	1·69	16·00	8·80	0·14	8·11	7·20	3·89	1·33
West Cuescomates	CH-05-13	WSU/CGEO	99°12′08″	19°04′30″		1·72							
West Cuescomates	CH-05-15	WSU/CGEO	99°12′17″	19°04′29″		1·71							
West Cuescomates	CH-05-12	WSU/CGEO	99°12′15″	19°04′30″	51·92	1·71	16·01	9·03	0·14	8·53	7·29	3·82	1·29
East Cuescomates	CH-08-1	WSU/CGEO	99°11′35″	19°04′27″	51·97	1·73	16·23	8·95	0·14	8·18	7·35	3·81	1·33
East Cuescomates	CH-08-2	WSU/CGEO	99°11′35″	19°04′27″	52·13	1·74	16·87	8·86	0·14	8·05	7·45	3·92	1·36
Main flow	MCH-06-10	WSU/CGEO	99°11′54″	19°01′43″	51·78	1·95	17·15	9·60	0·16	6·67	8·63	4·06	1·15
Main flow	ASC46B[2]	LaGatta (2003)	99°11′07″	19°01′19″									
Main flow	MCH-06-11	WSU/CGEO	99°10′36″	19°00′33″	51·67	1·92	17·01	9·73	0·16	6·98	8·58	3·95	1·13
Main flow	CH-08-4	WSU/CGEO	99°11′54″	19°03′17″	51·09	1·94	16·84	9·73	0·16	7·19	8·37	4·00	1·16
Main flow	CH-08-17	WSU/CGEO	99°08′32″	18°53′41″	50·52	1·93	16·48	10·13	0·16	8·20	8·02	3·96	1·12
Main flow	CH-08-18	WSU/CGEO	99°09′35″	18°55′47″	50·31	1·93	16·42	9·91	0·16	7·94	8·09	3·92	1·13
Old flow	CH-08-19	WSU/CGEO	99°10′46″	18°58′28″	49·57	1·95	16·89	10·30	0·16	8·32	8·95	3·76	0·92
Old flow	MCH-06-12	WSU/CGEO	99°10′54″	18°58′35″	49·98	1·96	17·01	10·20	0·16	7·96	9·16	3·78	0·92
Old flow	CH-09-11	WSU/CGEO	99°11′34″	18°59′55″	49·43	1·92	16·83	10·38	0·16	7·95	9·14	3·68	0·87

(continued)

Table 1: Continued

Sample no.	P_2O_5	LOI	Sum	Mg#[3]	Qtz[4]	Oliv[4]	Neph[4]	Sc	V	Ni	Cr	Co	Li	Be	Cs	Ba	U	Tl	Rb	Th	Nb
V. Chichinautzin																					
MCH-06-5	0·84	−0·20	100·2	63		0·0		19·9	143	133	208	30·1	15·1	2·34	1·01	471	1·04	0·17	28·9	3·47	33·1
CH-08-5	0·84		99·8	62		0·8		20·2	145	131	216	30·0	14·9	2·44	0·97	475	1·08	0·19	28·8	3·58	32·9
MCH-06-4	0·85	−0·24	99·9	63		0·1		20·4	145	130	215	29·7	13·7	2·36	1·01	473	1·05	0·17	28·9	3·48	33·4
MCH-06-2	0·90	−0·35	99·8	62	0·0			20·4	148	129	208	30·4	16·0	2·45	1·07	479	1·05	0·18	29·4	3·49	33·8
MCH-06-3	0·84	−0·14	100·0	62	0·2			20·6	147	127	204	29·9	12·5	2·45	0·99	471	1·05	0·16	28·7	3·48	33·5
MCH-06-1	0·90	−0·27	100·1	62	0·1			20·9	149	126	209	29·7	16·0	2·48	1·08	483	1·06	0·18	29·7	3·50	34·0
ASC1__S	0·97	0·00	99·4	60	1·4			21·9	149	100	199	27·7	16·4	2·56	1·06	490	1·08	0·17	30·0	3·59	34·5
ASC1__A	0·98		99·9	59	1·8			22·0	150	95	185	27·1	16·0	2·49	1·07	483	1·09	0·17	30·4	3·61	34·4
ASC1[2]																					
S11	1·00	0·37	99·6	58	2·6			21·7	145	76	188	25·3	16·8	2·41	1·11	509	1·14	0·17	31·5	3·80	35·5
S9	1·01	0·00	99·7	58	2·7			21·7	147	77	186	25·5	16·1	2·44	1·11	511	1·15	0·18	32·1	3·83	35·7
S10	1·01	0·18	99·7	58	3·0			22·0	148	67	176	24·2	15·4	2·37	1·13	513	1·16	0·18	32·3	3·84	35·8
MCH-06-7	0·91		99·9	58	3·4			21·1	145	59	161	23·9	17·2	2·49	1·20	511	1·17	0·19	32·3	3·86	35·0
S8	0·84	0·00	99·5	58	4·0			22·5	149	47	158	22·7	17·8	2·20	1·26	466	1·10	0·19	32·6	3·72	29·7
S3	0·86	−0·08	99·4	54	4·6			22·1	161	25	88	18·4	17·3	2·34	1·23	480	1·13	0·21	33·2	3·77	30·3
S7	0·86	−0·08	99·7	55	5·1			22·7	162	25	106	18·8	17·4	2·37	1·31	480	1·15	0·21	34·5	3·90	30·4
S6	0·85	0·13	99·7	54	4·7			22·6	161	24	100	18·6	17·5	2·38	1·30	477	1·14	0·21	34·2	3·85	30·2
S2	0·86	0·22	99·9	54	4·8			22·1	160	24	91	18·1	17·6	2·27	1·27	478	1·12	0·27	33·6	3·78	30·2
S4	0·86	−0·04	100·0	53	7·3			22·0	161	23	81	18·2	17·1	2·30	1·23	477	1·12	0·21	33·1	3·75	30·2
CH-07-18	0·80		100·3	55	8·1			21·3	152	23	92	18·9	17·9	2·35	1·34	501	1·12	0·21	34·1	3·81	29·9
S5	0·87	−0·11	99·5	53	4·2			22·1	166	23	80	18·0	17·7	2·32	1·24	481	1·13	0·21	33·5	3·78	30·4
S1	0·63	0·04	99·5	51	6·4			17·8	144	8	13	15·7	18·6	2·20	1·23	418	1·06	0·21	29·6	3·36	21·7
CH-07-16	0·61		100·1	52	6·6			16·8	137	8	15	15·4	16·6	2·07	1·22	421	1·02	0·28	29·5	3·25	20·8
CH-07-17	0·61		99·9	52	6·4			17·5	137	8	16	15·3	16·6	2·08	1·18	418	1·02	0·20	28·8	3·27	21·0
CH-07-15	0·62		99·4	51	6·3			17·6	140	7	14	15·5	16·1	2·14	1·21	427	1·03	0·27	29·3	3·27	21·7
Texcal Flow																					
CH-05-16	0·56	−0·18	100·2	69		8·9		21·5	157	179	256	35·2	11·9	2·00	0·88	371	0·92	0·14	26·1	3·15	26·1
S12B	0·58		99·7	69		8·3		22·4	157	187	303	35·8	12·4	1·93	0·86	358	0·90	0·14	25·6	3·10	25·3
CH-05-13	0·58					n.a.		21·2	152	192	257	36·5	9·5	2·02	0·86	374	0·92	0·18	25·5	3·14	26·0
CH-05-15	0·60					n.a.		21·0	152	183	241	35·0	11·6	1·95	0·88	371	0·92	0·14	26·1	3·14	25·8
CH-05-12	0·55	0·26	99·4	70		9·5		21·2	152	203	266	37·1	11·8	1·95	0·86	364	0·91	0·11	25·2	3·10	25·7
CH-08-1	0·56		99·4	69		8·6		20·6	148	185	289	35·2	10·4	1·99	0·83	363	0·91	0·13	24·9	3·10	25·1
CH-08-2	0·55		100·2	69		10·4		20·9	151	181	282	35·1	10·8	2·00	0·84	368	0·92	0·14	25·5	3·14	25·5
MCH-06-10	0·55	−0·40	100·7	63		10·7		25·6	175	85	215	32·6	11·3	1·99	0·53	275	0·68	0·07	18·8	2·27	24·0
ASC46B[2]																					
MCH-06-11	0·53	−0·27	100·7	63		10·5		25·5	173	91	228	33·2	11·3	1·95	0·65	271	0·74	0·10	19·5	2·27	23·7
CH-08-4	0·54		100·0	64		12·8		23·9	162	99	247	33·0	10·5	1·94	0·62	262	0·75	0·10	19·4	2·25	23·4
CH-08-17	0·51		100·0	66		16·5		22·4	157	145	289	37·3	10·4	1·81	0·46	242	0·63	0·07	16·8	2·14	22·8
CH-08-18	0·54		99·4	66		15·3		23·7	163	138	295	37·1	10·6	1·96	0·58	259	0·75	0·09	19·1	2·26	23·7
CH-08-19	0·36		100·1	66		17·5	0·8	25·7	187	132	265	40·8	9·2	1·75	0·44	172	0·58	0·11	13·5	1·73	18·3
MCH-06-12	0·35	−0·32	100·5	65		16·5	0·5	26·5	192	119	252	39·8	9·2	1·73	0·48	174	0·41	0·07	14·1	1·74	19·0
CH-09-11	0·35		99·7	65		16·7	0·3	26·1	196	123	252	40·1	8·1	1·66	0·37	170	0·53	0·05	14·0	1·66	17·3

(continued)

Table 1: Continued

Sample no.	Ta	La	Ce	Pb	Pr	Sr	Nd	Sm	Hf	Zr	Eu	Gd	Tb	Dy	Y	Ho	Er	Yb	Lu
V. Chichinautzin																			
MCH-06-5	1·76	37·4	79·9	6·92	10·2	535	42·3	8·79	7·44	387	2·54	8·16	1·22	6·90	39·8	1·37	3·78	3·45	0·53
CH-08-5	1·77	38·0	82·3	6·89	10·4	539	43·1	8·87	7·54	392	2·61	8·31	1·26	7·13	40·9	1·42	3·88	3·59	0·54
MCH-06-4	1·77	37·6	80·7	6·97	10·4	540	43·0	8·94	7·52	391	2·56	8·26	1·24	7·03	40·4	1·39	3·83	3·50	0·54
MCH-06-2	1·76	39·7	85·5	7·30	11·0	524	45·7	9·40	7·79	410	2·68	8·69	1·29	7·31	42·2	1·44	3·99	3·66	0·56
MCH-06-3	1·78	37·4	80·6	6·87	10·3	542	42·7	8·91	7·53	383	2·57	8·24	1·24	7·00	40·4	1·39	3·83	3·52	0·55
MCH-06-1	1·78	40·1	85·6	7·34	11·1	525	46·0	9·50	7·88	414	2·69	8·76	1·31	7·36	42·7	1·46	4·04	3·69	0·57
ASC1__S	1·79	42·0	94·7	7·69	11·7	525	48·6	9·87	8·12	428	2·84	9·21	1·39	7·74	44·3	1·54	4·22	3·88	0·59
ASC1__A	1·83	41·7	95·7	7·86	11·7	522	48·5	9·75	8·11	433	2·85	9·20	1·39	7·77	44·2	1·52	4·22	3·90	0·59
ASC1[2]																			
S11	1·83	43·8	98·8	7·99	12·2	517	50·5	9·97	8·23	435	2·90	9·36	1·42	7·86	44·8	1·55	4·24	3·94	0·60
S9	1·86	44·5	100·5	8·13	12·3	517	50·9	10·09	8·33	443	2·91	9·45	1·43	7·89	45·1	1·56	4·26	3·96	0·60
S10	1·88	44·5	100·9	8·16	12·3	522	50·9	10·13	8·32	444	2·92	9·49	1·43	7·96	45·1	1·56	4·28	3·98	0·60
MCH-06-7	1·80	43·9	95·0	7·33	12·1	517	49·2	10·13	8·02	436	2·81	9·18	1·36	7·90	43·3	1·52	4·17	3·83	0·58
S8	1·57	38·9	86·9	7·73	10·7	486	44·6	9·04	7·43	386	2·58	8·49	1·29	7·19	41·6	1·44	3·96	3·67	0·56
S3	1·61	40·1	90·2	8·11	11·1	512	46·1	9·29	7·72	398	2·68	8·80	1·34	7·49	43·3	1·48	4·14	3·89	0·58
S7	1·61	40·3	90·6	8·25	11·2	502	46·2	9·26	7·77	397	2·70	8·81	1·34	7·52	43·3	1·48	4·11	3·88	0·58
S6	1·58	39·8	89·3	8·18	11·0	502	45·7	9·18	7·64	392	2·65	8·66	1·32	7·39	42·6	1·47	4·06	3·81	0·58
S2	1·58	39·8	88·4	8·22	11·0	505	45·7	9·24	7·67	391	2·64	8·70	1·32	7·40	42·9	1·48	4·08	3·83	0·58
S4	1·59	39·9	87·9	8·11	11·0	510	45·7	9·25	7·72	397	2·67	8·72	1·33	7·46	43·1	1·47	4·11	3·87	0·59
CH-07-18	1·58	39·6	87·8	7·87	10·8	496	45·0	9·19	7·65	387	2·63	8·68	1·32	7·34	42·0	1·46	4·09	3·75	0·58
S5	1·61	40·2	90·0	8·06	11·2	504	46·3	9·32	7·78	396	2·67	8·82	1·34	7·49	43·4	1·49	4·11	3·89	0·59
S1	1·16	30·7	68·5	7·31	8·6	518	35·8	7·56	6·56	327	2·22	7·16	1·10	6·24	36·6	1·26	3·52	3·31	0·51
CH-07-16	1·12	29·4	63·5	7·11	8·1	508	33·9	7·31	6·46	305	2·20	6·92	1·08	5·96	35·0	1·19	3·40	3·25	0·49
CH-07-17	1·14	30·4	66·2	6·99	8·3	509	34·9	7·35	6·52	307	2·18	7·20	1·11	6·17	35·9	1·23	3·44	3·25	0·51
CH-07-15	1·17	30·6	67·9	7·12	8·5	510	36·0	7·58	6·55	317	2·23	7·25	1·12	6·24	36·4	1·26	3·55	3·34	0·51
Texcal Flow																			
CH-05-16	1·45	26·7	57·6	5·16	7·3	548	30·7	6·61	5·58	272	2·01	6·35	0·97	5·59	32·1	1·12	3·07	2·86	0·43
S12B	1·41	26·2	56·5	5·06	7·2	537	30·3	6·50	5·45	268	1·98	6·24	0·97	5·52	31·7	1·11	3·06	2·83	0·43
CH-05-13	1·43	26·6	58·7	5·32	7·3	538	30·6	6·58	5·53	271	1·99	6·29	0·97	5·56	32·0	1·11	3·05	2·84	0·43
CH-05-15	1·44	26·6	57·5	5·21	7·3	539	30·9	6·57	5·56	273	2·00	6·34	0·97	5·58	32·1	1·11	3·08	2·85	0·43
CH-05-12	1·42	26·1	57·8	5·19	7·2	534	30·2	6·50	5·48	270	1·97	6·23	0·96	5·51	31·7	1·10	3·03	2·82	0·43
CH-08-1	1·41	26·5	56·4	5·24	7·2	529	29·9	6·42	5·47	269	1·97	6·20	0·95	5·50	31·6	1·10	3·01	2·80	0·42
CH-08-2	1·44	26·7	57·3	5·06	7·3	540	30·4	6·47	5·53	272	1·99	6·31	0·96	5·61	32·2	1·13	3·07	2·85	0·43
MCH-06-10	1·37	21·8	49·2	4·16	6·4	488	27·2	6·24	5·18	252	1·99	6·32	1·00	5·86	34·2	1·19	3·27	3·04	0·47
ASC46B[2]																			
MCH-06-11	1·36	21·7	48·5	3·91	6·3	485	27·1	6·20	5·19	251	1·98	6·30	1·00	5·84	33·9	1·19	3·28	3·06	0·47
CH-08-4	1·36	21·4	47·3	3·68	6·1	480	26·4	5·97	5·04	253	1·94	6·11	0·96	5·67	32·8	1·15	3·16	2·95	0·45
CH-08-17	1·36	20·4	45·3	3·29	5·8	488	24·8	5·66	4·87	241	1·85	5·82	0·91	5·37	30·7	1·08	2·97	2·73	0·41
CH-08-18	1·40	21·6	47·7	3·58	6·2	491	26·4	6·01	5·14	259	1·95	6·16	0·96	5·71	32·9	1·16	3·16	2·96	0·45
CH-08-19	1·11	16·2	36·6	2·54	4·8	509	20·8	5·05	4·31	208	1·72	5·57	0·89	5·38	31·2	1·10	3·03	2·80	0·43
MCH-06-12	1·14	16·4	37·8	2·58	4·9	520	21·4	5·25	4·39	208	1·76	5·67	0·92	5·49	31·7	1·11	3·09	2·88	0·43
CH-09-11	1·06	15·4	35·3	2·55	4·6	498	20·4	5·02	4·25	207	1·70	5·51	0·89	5·35	31·0	1·09	3·03	2·79	0·42

(continued)

Table 1: Continued

Sample no.	$^{87}Sr/^{86}Sr$[5]	2 STEM	$^{143}Nd/^{144}Nd$[5]	2 STEM	$^{87}Sr/^{86}Sr$[6]	2 STEM	$^{143}Nd/^{144}Nd$[6]	2 STEM
V. Chichinautzin								
MCH-06-5					0·704208	10	0·512757	10
CH-08-5								
MCH-06-4								
MCH-06-2								
MCH-06-3	0·704203	8	0·512775	8				
MCH-06-1	0·704353	8	0·512749	6				
ASC1__S	0·704378	8	0·512757	7				
ASC1__A								
ASC1[2]								
S11	0·704490	10	0·512754	7				
S9	0·704493	9	0·512733	6				
S10								
MCH-06-7								
S8	0·704528	8	0·512743	6				
S3	0·704399	7	0·512745	8				
S7	0·704489	7	0·512734	7				
S6								
S2	0·704475	7	0·512743	6				
S4	0·704392	7	0·512746	6	n.d.		0·512736	18
CH-07-18	0·704506	10	0·512733	7				
S5	0·704386	7	0·512751	10				
S1	0·704055	10	0·512801	7	0·704050	8	0·512796	16
CH-07-16	0·704057	6	0·512799	6				
CH-07-17								
CH-07-15	0·704100	6	0·512795	6				
Texcal Flow								
CH-05-16	0·703805	6	0·512824	10	0·703795	12	0·512825	14
S12B								
CH-05-13								
CH-05-15								
CH-05-12	0·703811	7	0·512818	8				
CH-08-1								
CH-08-2								
MCH-06-10								
ASC46B[2]								
MCH-06-11	0·703607	8	0·512866	8				
CH-08-4	0·703592	10	0·512884	6				
CH-08-17					0·7034554	10	0·512910	18
CH-08-18								
CH-08-19	0·703061	9	0·512992	6				
MCH-06-12	0·703087	8	0·512987	6	0·7030556	10	0·512982	14
CH-09-11	0·703053	9	0·512994	6				

Major element abundances in oxide wt %, trace element abundances in ppm; n.d., not determined. Total Fe given as Fe_2O_3. Selected data for the following samples have been reported by Straub *et al*. (2011): MCH06-5, S9, S8, S4, S1, MCH06-12, CH08-17, MCH06-11, CH05-6. The data reported are: SiO_2, FeO*, MgO, Ni, Sr, Nb, La, Gd, Y, Yb, and Nd isotope ratios.

[1]Laboratory where major and trace elements were obtained (Harvard, Langmuir Laboratory; WSU, Washington State University; CGEO, Centro de Geociencias).

[2]All data for samples ASC1 and ASC45B are from LaGatta (2003).

[3]Bulk rock Mg#, calculated assuming 18% ferric Fe.

[4]CIPW norm: Qtz, quartz-normative; Oliv, olivine-normative; Neph, nepheline-normative. Calculation with program created by K. Hollocher at the Union College of Schenectady (http://www.union.edu/PUBLIC/GEODEPT/COURSES/petrology/norms.htm).

[5]Sr and Nd isotope analyses from Institute of Earth Sciences, Taipei, Taiwan.

[6]Sr and Nd isotope analyses from Lamont–Doherty Earth Observatory, Palisades, NY, USA.

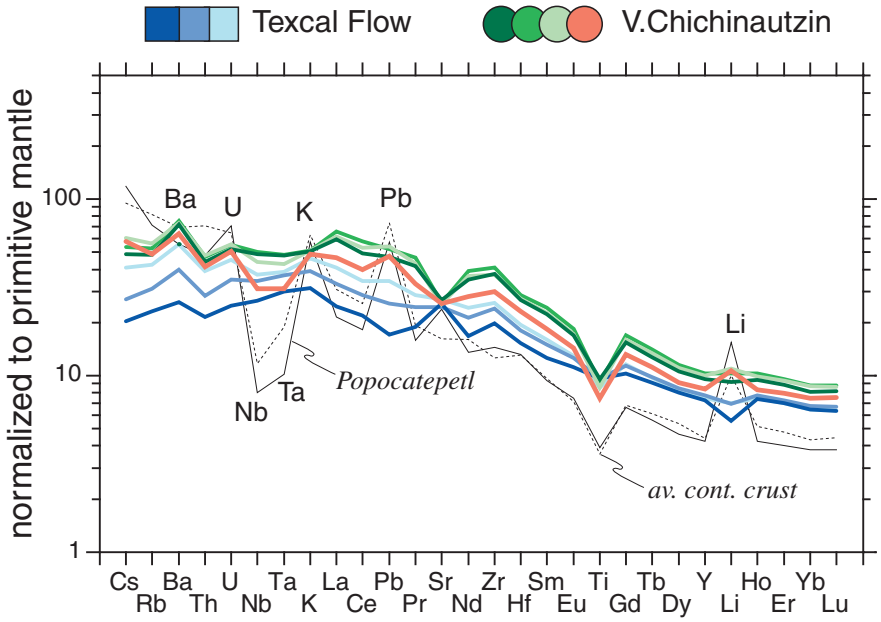

Fig. 3. Incompatible trace element abundances in the Texcal Flow and V. Chichinautzin normalized to primitive mantle after McDonough & Sun (1995). The average of each eruptive unit is compared with average Popocatepetl volcanic rocks (continuous line; Schaaf *et al.*, 2005) and bulk continental crust (dashed line; Rudnick & Gao, 2002).

and V. Chichinautzin are higher and range from ~1·9 to 2·8. Like the pyrolite, however, the heavy REE (HREE) patterns are flat, with only marginally increased $Ho/Lu_n = 1·1–1·2$. Texcal Flow and V. Chichinautzin thus lack 'garnet-signatures' that might point to the involvement of silicic partial slab melts ('adakites') in their petrogenesis (e.g. Kay, 1978; Defant & Drummond, 1990; Gómez-Tuena *et al.*, 2007*a*). This agrees with the mostly low SiO_2 <56 wt % (adakites >56 wt %) of the Texcal Flow and V. Chichinautzin, as well as the high Y (31–45 ppm, adakites <18 ppm) and low Sr/Y (11–17, adakites >50).

Sr and Nd isotope ratios

The ratios of $^{87}Sr/^{86}Sr = 0·70305–0·70453$ and $^{143}Nd/^{144}Nd = 0·51273–0·51299$ of the Texcal Flow and V. Chichinautzin largely coincide with previously reported data (Siebe *et al.*, 2004*a*). However, our extended dataset reveals for the first time that the Sr and Nd isotope ratios also differ systematically in the various eruptive units at each volcano (Fig. 5). The only exceptions are the V. Chichinautzin shield and cone lavas, which have similar Nd and Sr isotope ratios. $^{87}Sr/^{86}Sr$ and $^{143}Nd/^{144}Nd$ also correlate with bulk-rock SiO_2. In the Texcal Flow, SiO_2 increases with increasing $^{87}Sr/^{86}Sr$ and decreasing $^{143}Nd/^{144}Nd$. At V. Chichinautzin, this trend continues only in the distal flows, but reverses in the shield and cone lavas, so that the youngest and most silica-rich summit lavas have the least radiogenic Sr and most radiogenic Nd of all V. Chichinautzin samples. The Sr and Nd isotope data further corroborate the inference that the Texcal Flow and V. Chichinautzin magma series are not related by fractional crystallization, and must be derived from a heterogeneous source.

Composition of olivine phenocrysts

Melt heterogeneity as recorded by olivine phenocrysts

Olivine is ubiquitous as a phenocryst phase in Texcal Flow and V. Chichinautzin lavas (Straub *et al.*, 2011*a*). Invariably, the olivines show zoning patterns that must have been produced by melt mixing. Olivine zonation ranges from normal to inverse and complex (normal and inverse) zoning (e.g. sample S8, Fig. 6; see also Electronic Appendix Table 1). Moreover, most samples have multiple olivine populations that cannot be related to each other by fractional crystallization (Straub *et al.*, 2008, 2011*a*). Overall, olivine zoning and diversity increase with increasing melt SiO_2 and are more prevalent in V. Chichinautzin than in the Texcal Flow. The olivines of the most primitive old Texcal Flow (sample MCH06-12) exhibit only normal zoning, and melt mixing is indicated only by the straight trend in the Fo–Ni diagram, which differs from the curved trends produced by fractional crystallization (e.g. Fig. 7).

The Mg# of the melts in equilibrium with the olivines ($=Mg\#_{oliv}$) can be calculated using the mineral/melt exchange coefficient $K_{D\,Fe/Mg}^{oliv/melt}$ of Roeder & Emslie (1970). When compared with the whole-rock Mg#, these data show that the olivines in a given sample (small grey dots) extend well above and below the equilibrium band

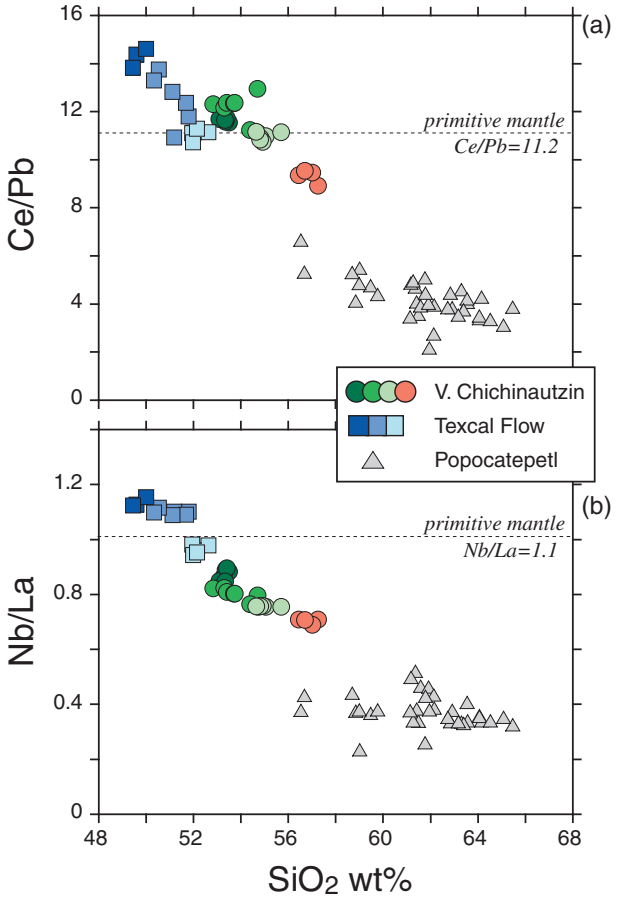

Fig. 4. (a, b) Whole-rock Ce/Pb and Nb/La vs SiO_2 (wt %) for the Texcal Flow and V. Chichinautzin compared with Popocatepetl volcanic rocks (Schaaf *et al.*, 2005).

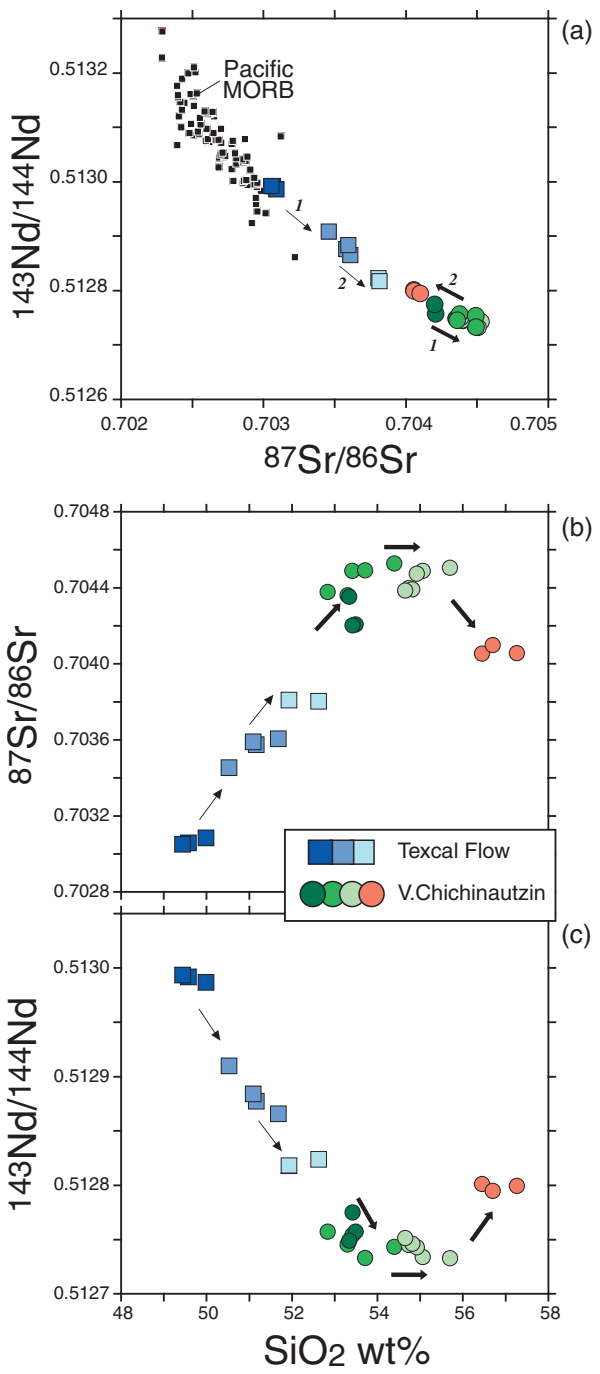

Fig. 5. (a–c) Whole-rock $^{87}Sr/^{86}Sr$ and $^{143}Nd/^{144}Nd$ and SiO_2 variation in the Texcal Flow and V. Chichinautzin lavas. Pacific MORB from GeoROC (2011).

(Fig. 8), with an average of 7 ± 3 $Mg\#_{oliv}$ difference in single samples. This range reflects the hybrid nature of Texcal Flow and V. Chichinautzin magmas, which consist of two or more component melts, with slightly different melt Mg#, that mixed incompletely prior to eruption [see detailed discussion by Straub *et al.* (2008, 2011*a*)]. However, the average $Mg\#_{oliv}$ of all olivines in a single sample falls within, or close to, the equilibrium range (Fig. 8). This means that the bulk-rock represents reasonably well the average of the component melts that crystallize the olivines (Straub *et al.*, 2011*a*).

There is no evidence that the olivine Fo content within a single sample was controlled by different melt oxygen fugacity based on Cr-spinel inclusions in the olivines of V. Chichinautzin samples ASCLA and ASCLS (Electronic Appendix Table 2). These two samples were taken from the same location, and both samples exhibit a bimodal olivine distribution with maxima at $\sim Fo_{80}$ (low-Fo olivines) and $\sim Fo_{83\cdot5}$ (high-Fo olivines), respectively (Straub *et al.*, 2008). The maxima plot above and below the equilibrium value for the bulk-rock that corresponds to $\sim Fo_{81}$. The Fe_2O_3/FeO_2 of Cr-spinel inclusions is protected by the olivine host and reflects the ferric/ferrous iron ratio of the melt at the time the Cr-spinel grew (Maurel & Maurel, 1982; Gurenko *et al.*, 1996). Cr-spinels from both

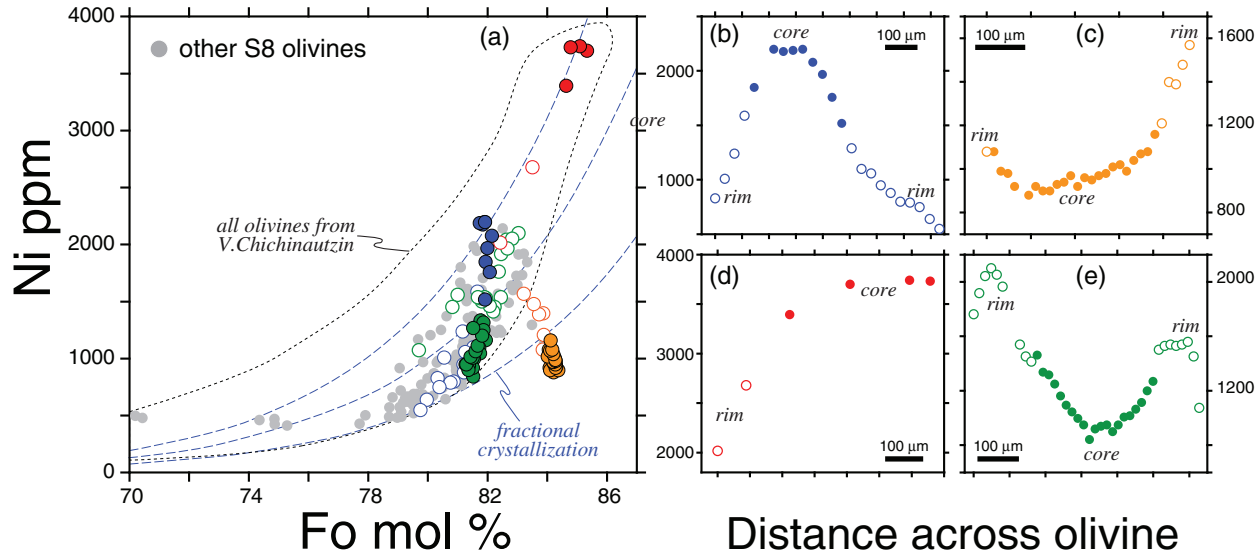

Fig. 6. (a) Variation of Ni vs Fo mol % in olivines of sample S8 (V. Chichinautzin). compared with all olivines from V. Chichinautzin [data in Electronic Appendix Table 1 and given by Straub *et al.* (2008, 2011*a*)]. Fractional crystallization lines calculated after Straub *et al.* (2011*a*). Filled circles, olivine cores; open circles, olivine rims. Straight trends for single olivines that cross fractional crystallization trajectories should be noted. Such trends are typical for melt mixing (b–e). Normal and inverse zoning patterns of selected olivine phenocrysts as in (a).

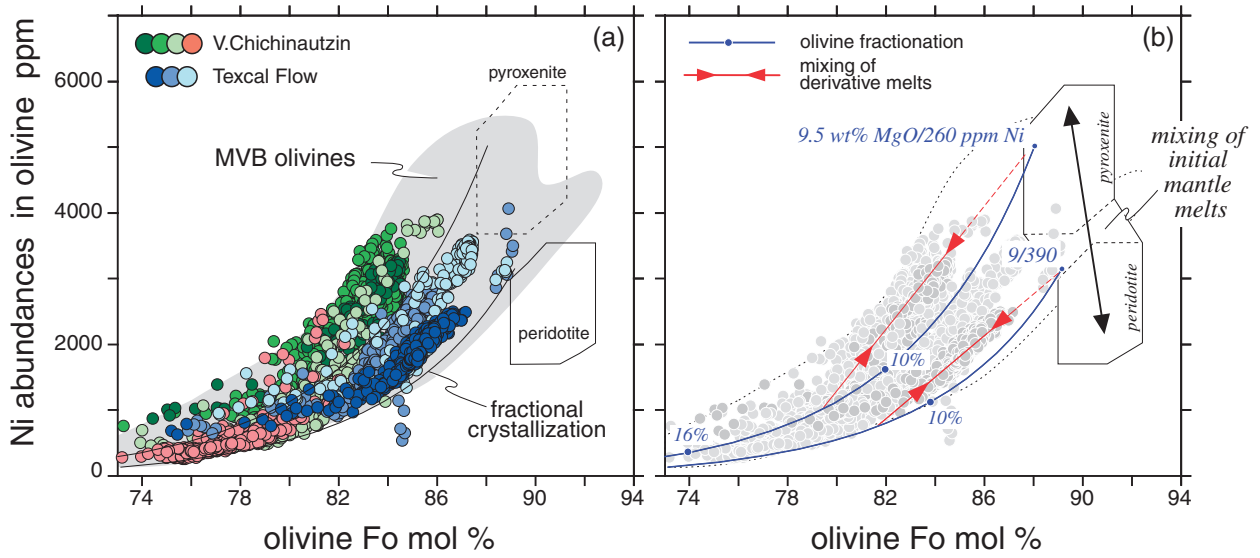

Fig. 7. Ni (ppm) vs Fo (mol %) of olivine phenocrysts (core compositions) from the Texcal Flow and V. Chichinautzin. (a) Olivine data from Straub *et al.* (2008, 2011*a*). Grey field denotes other central MVB olivines. Fields labeled 'pyroxenite' and 'peridotite' indicate olivine composition in equilibrium with initial partial melts of pyroxenite and peridotite after Straub *et al.* (2011*a*). (b) Interpretation of olivine compositions after Straub *et al.* (2011*a*). Few olivines are in equilibrium with initial mantle melts (hybrids of pyroxenite and peridotite melts), and most olivines crystallize from derivative melts. Large near-vertical arrow (to the right) indicates mixing between pyroxenite and peridotite initial, high-Mg# component melts. Bold curved lines with dots delineate olivine fractionation trends, with percentage of olivine fractionation given in italics. The MgO and Ni content of the initial bulk melt composition is shown at the start of the fractional crystallization curves. Bold lines with inward pointing arrows indicate recharge mixing. [For discussion see text and Straub *et al.* (2011*a*).]

low-Fo and high-Fo olivines yield identical ratios of $Fe^{3+}/\sum Fe$ in the melt; that is, $0{\cdot}16 \pm 0{\cdot}03$ (2σ, $n = 62$ Cr-spinels) and $0{\cdot}18 \pm 0{\cdot}03$ (2σ, $n = 39$), respectively. These are identical, within error, and argue against the existence of melt batches with different melt oxygen fugacities. Notably, these values are also similar to the melt $\sum Fe^{3+}/Fe^{2\pm} = 0{\cdot}13 \pm 0{\cdot}04$ (2σ) obtained from Cr-spinel inclusions in the forsteritic olivines (~Fo_{89}) of Popocatepetl (Straub &

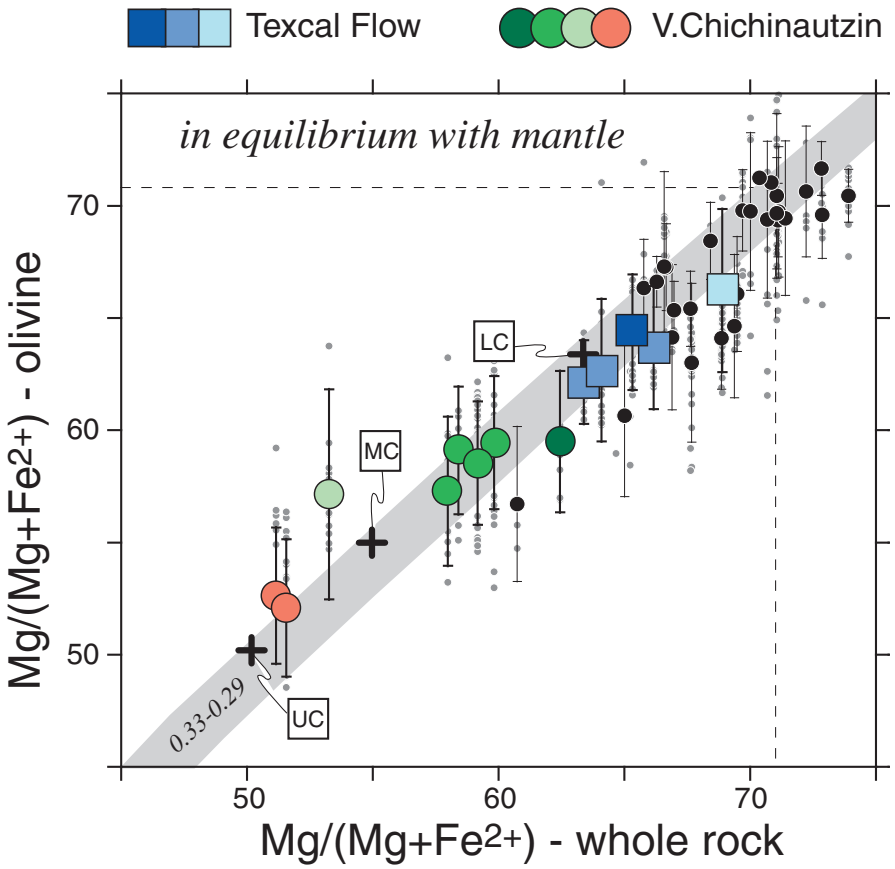

Fig. 8. Whole-rock Mg# vs Mg# calculated from the average olivine composition per sample based on the mineral/melt exchange coefficient $KD_{Fe/Mg}^{oliv/melt}$ of Roeder & Emslie (1970). A $KD_{Fe/Mg}^{oliv/melt} = 0{\cdot}32$ was used and a ferric/ferrous ratio of $0{\cdot}18 \pm 0{\cdot}04$ [as given by Straub *et al.* (2008, 2011*a*)]. Grey band indicates equilibrium for the exchange coefficient $KD_{Fe/Mg}^{oliv/melt} = 0{\cdot}29$–$0{\cdot}33$; the regression through all the samples is $y = 1{\cdot}02\,x$, $R^2 = 0{\cdot}89$ (forced through the origin). Total error bars are 2 standard deviations of average Mg# obtained from all single olivine analyses (core and rims) per sample. Small grey dots are averages of single olivine grains. Larger black circles are the averages of other samples from the central MVB (Straub *et al.*, 2011*a*). The fit with the equilibrium line improves with the number of olivines analysed per sample. Average of upper (UC), middle (MC) and lower (LC) continental crust after Rudnick & Gao (2002).

Martin-Del Pozzo, 2001) and melt $\sum Fe^{3+}/Fe^{2+} = 0{\cdot}18 \pm 0{\cdot}04$ (2σ) obtained from Cr-spinels from a broader spectrum of central MVB magmas (Straub *et al.*, 2008), all of which suggest that the central MVB magmas have similar melt oxygen fugacities.

High-Ni olivines

The olivines of Texcal Flow and V. Chichinautzin are 'high-Ni olivines', which have Ni contents that are well above those of MORB olivines at $<Fo_{90}$ (Fig. 7, Straub *et al.*, 2011*a*). 'High-Ni' olivines thus have higher Ni contents than feasible for olivines that crystallize from partial melts of peridotite. The high-Ni olivines have been interpreted to result from melting of 'reaction pyroxenite' rather than of a peridotite mantle source (Sobolev *et al.*, 2005; Herzberg, 2011; Straub *et al.*, 2011*a*). Sobolev *et al.* (2005) proposed that these 'reaction pyroxenites' form through infiltration of silicic melts derived from subducted eclogite into mantle peridotite. Infiltration of silicic slab components (silica-rich fluids or hydrous melts) into a peridotite subarc mantle is a natural consequence of subduction recycling (e.g. Kelemen, 1995; Hermann *et al.*, 2006). Indeed, high-Ni olivines are ubiquitous in the central MVB (Straub *et al.*, 2008, 2011*a*) where slab influence is evident in magma chemistry throughout the belt (e.g. LaGatta, 2003; Martinez-Serrano *et al.*, 2004; Schaaf *et al.*, 2005). An intriguing aspect of 'reaction pyroxenites' is that they may produce a broader spectrum of basaltic to dacitic melts dependent on their bulk silica content (silica-deficient vs quartz-normative) (Kogiso *et al.*, 2004; Straub *et al.*, 2011*a*). The presence of high-Ni olivines in the Texcal Flow and V. Chichinautzin magmas thus suggests that melt-rock reaction processes in the sub-arc mantle may play an important role in their petrogenesis.

DISCUSSION

The SiO_2 contents of the Texcal Flow and V. Chichinautzin magmas clearly exceed those of initial partial melts of peridotite mantle, which have melt $SiO_2 \leq 50$ wt % (Langmuir

et al., 1992). Any petrogenetic model must account for the high melt SiO_2 and its systematic variation with $^{87}Sr/^{86}Sr$ and $^{143}Nd/^{144}Nd$.

No evidence for melt silica increase by fractional crystallization

The covariation of melt SiO_2 with $^{87}Sr/^{86}Sr$ and $^{143}Nd/^{144}Nd$ precludes the possibility that melt SiO_2 increases by closed-system fractional crystallization from a common basaltic parental melt (Fig. 5). This result is remarkable as some of the major element trends resemble those predicted for fractional crystallization (Fig. 2). For example, the increase and decrease of P_2O_5 with SiO_2 is commonly linked to apatite fractionation (e.g. Green & Watson, 1982), and the decrease of TiO_2 and Fe_2O_3 with increasing silica has been linked to the fractionation of Fe–Ti-oxides from the melt (e.g. Plank & Langmuir, 1988).

On the other hand, the melt SiO_2 increase may be due to more complex fractional crystallization processes. For example, early 'cryptic crystallization' may produce silica-rich derivative melts from multiple low-SiO_2 ($\leq$49 wt %) mantle-derived magmas with different $^{87}Sr/^{86}Sr$ and $^{143}Nd/^{144}Nd$. Cryptic crystallization refers to phases that influence melt evolution without being physically observed (Langmuir, 1989; Davidson *et al.*, 2007). In the central MVB, olivines mostly crystallize at mid- to upper crustal levels based on the H_2O and CO_2 contents of melt inclusions (Cervantes & Wallace, 2003; Roberge *et al.*, 2009). Hence, early cryptic crystallization may occur in the lower crust (>0·8 GPa), and possibly even in the mantle (Yogodzinski *et al.*, 1995). Given the crystallization temperatures of the olivines [calculated from average olivine and bulk-rock compositions after Roeder & Emslie (1970), with data from Straub *et al.* (2011*a*)], early crystallization must take place at temperatures >1150–1200°C.

To test whether 'cryptic phases' influence melt evolution, equilibrium olivine was added to the bulk-rock in 0·1% steps until equilibrium with Fo_{88} olivine (maximum Fo observed). Although this correction is a simplification (as the bulk-rocks are hybrids rather than liquids), the approach is feasible because only small amounts of olivine need to be added (on average 7·6 ± 4%), and hence the effect on incompatible elements is negligible. The correction mostly affects melt MgO, but even melt FeO and SiO_2 change only within <3% relative, as $Kd_{Si}^{oliv/melt}$ (~0·8) and $Kd_{Fe}^{oliv/melt}$ (~1–2) are close to unity. All other elements are considered as perfectly incompatible. The corrected elements are denoted by the subscript '88' hereafter.

The corrected melt compositions display a significant range from 49·0 to 55·2 Si_{88} wt %, but no correlation with Si_{88} emerges that points to early cryptic phases (Fig. 9). For example, garnet and amphibole are ruled out, because (1) Ho/Lu does not increase with melt SiO_2, (2) the most silicic melts have the lowest Ho/Lu observed, and (3) the highest La/Yb is not coupled with the lowest Gd/Yb (Davidson *et al.*, 2007). Plagioclase fractionation is unsupported because Sr_{88} barely varies, and does not correlate with Si_{88} (or Ca_{88}, Al_{88} or Na_{88}). Magnetite loss would increase melt Mg# with increasing SiO_2, but the silicic V. Chichinautzin magmas have lower Mg# values than those of the Texcal Flow. Apatite is not stable at the relevant temperatures and pressures (Green & Watson, 1982). K_2O behaves incompatibly towards all possible cryptic phases (including amphibole), but K_{88} increases with increasing Si_{88} only in the Texcal Flow, and even slightly decreases at V. Chichinautzin, so that the most silicic melts do not have the highest K_{88}, as expected for fractional crystallization.

The exception are ortho- and clinopyroxenes, which cannot be detected by incompatible trace elements and are stable at lower crustal pressures (Weaver *et al.*, 2011; Weber *et al.*, 2011). However, orthopyroxenes (~52–53 wt % SiO_2) are more silica-rich than basaltic mantle melts, and cannot increase melt SiO_2 from $\leq$49 wt %. Clinopyroxenes have less SiO_2 (~49–50 wt %), but are so similar to the melt SiO_2 that only the loss of large a quantity (>50%) may significantly increase melt SiO_2. However, there are no negative correlations of Ca_{88} and Ca_{88}/Al_{88} with Si_{88} in the single eruptive units, which would have to occur if clinopyroxene was to increase melt SiO_2 in the eruptive units.

Even if early cryptic crystallization did occur, the problem remains of how multiple, independently evolving melt batches would eventually converge to form the regular trends observed. For the same reason, we consider it as unrealistic that the simultaneous crystallization of multiple phases, mutually cancelling out their signatures, was responsible for the regular trends of SiO_2 and other major element oxides. In summary, processes other than fractional crystallization must control the increase of melt SiO_2 at Texcal Flow and V. Chichinautzin.

No evidence for crustal contamination

In view of the ubiquitous evidence for melt mixing in the central MVB magmas (e.g. Nixon, 1988*a*, 1988*b*; Straub & Martin-Del Pozzo, 2001; Straub *et al.*, 2008), the mixing of basaltic mantle melts with silicic crustal material seems to be a straightforward way to account for the melt silica increase with time. Moreover, the Texcal Flow and V. Chichinautzin volcanic rocks often contain clots of millimeter- to centimeter-sized recrystallized quartz, which are widely considered as visual evidence of entrained crustal material (e.g. Siebe *et al.*, 2004*a*). However, the amount of crustal material needed to increase melt SiO_2 is substantial. Assuming that the SiO_2 increase at Texcal Flow and V. Chichinautzin is due to mixing of a silicic crustal component ($\geq$57% wt % SiO_2 and $\leq$3 wt % MgO) with a

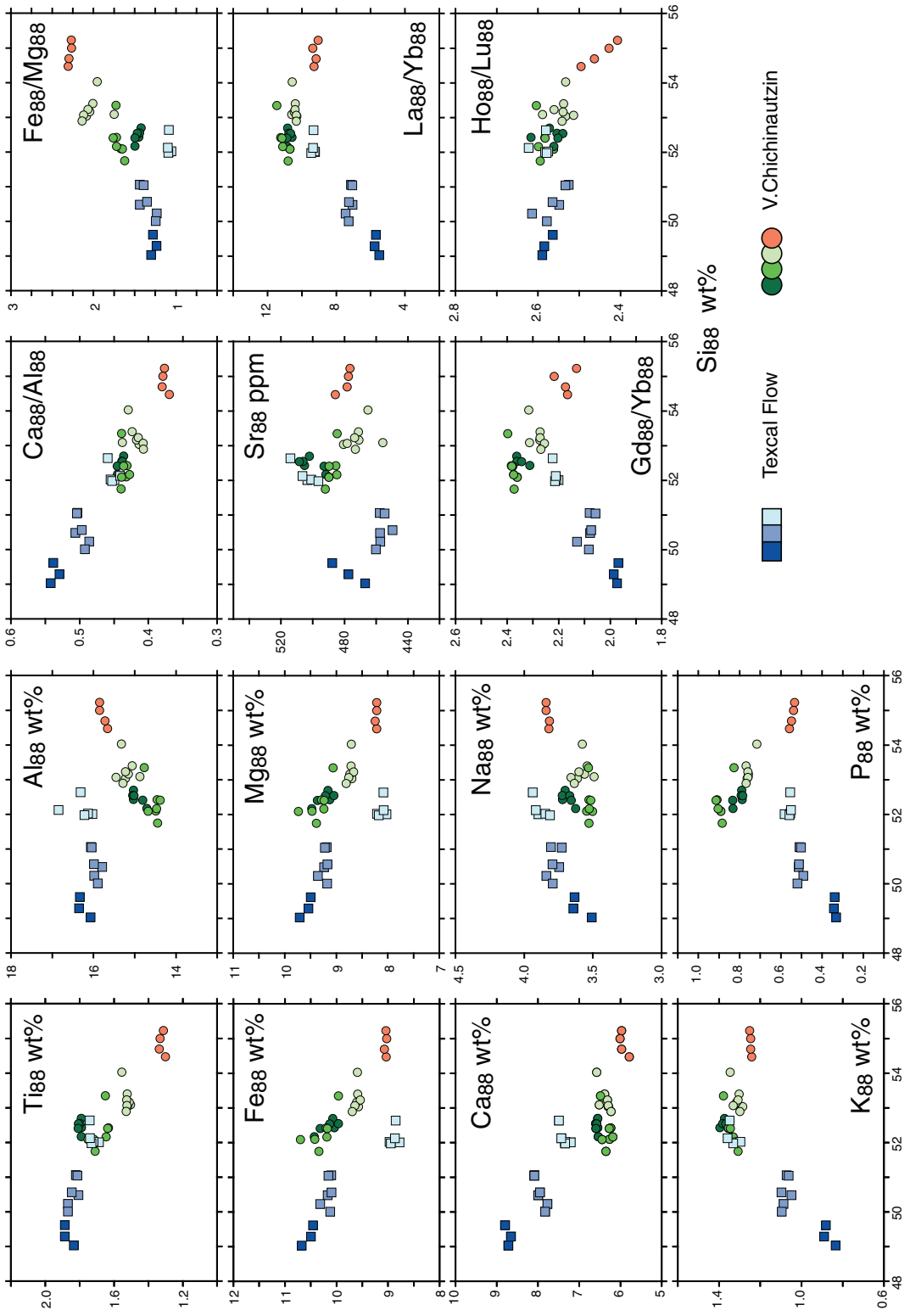

Fig. 9. Fractionation-corrected trends of major element oxides and selected trace elements. Correction was done by adding calculated equilibrium olivine to the bulk rock (or subtracting olivine in a few cases) in 0·1% steps until equilibrium with Fo_{88} was achieved.

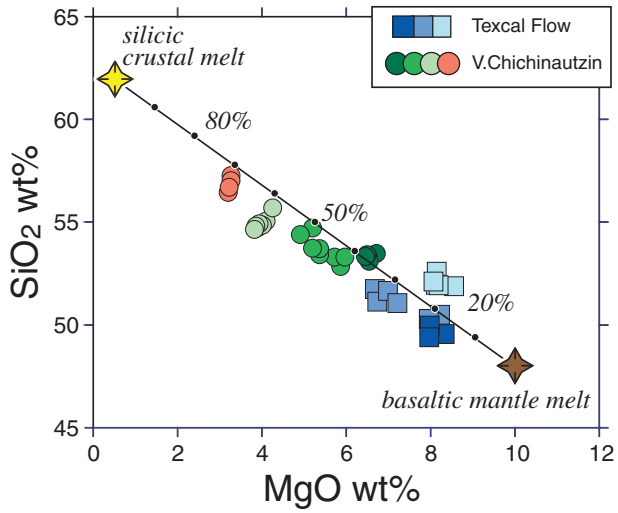

Fig. 10. Whole-rock SiO_2 wt % vs MgO wt % for V. Chichinautzin and the Texcal Flow. Mixing end-members are indicated by stars. Mixing line is calculated with a mantle melt of $SiO_2 = 48$ wt % and MgO = 10 wt %, and a crustal component with the highest possible melt $SiO_2 = 62$ wt %, and MgO = 0·5 wt %. Dots on mixing line denote 10% mixing increments.

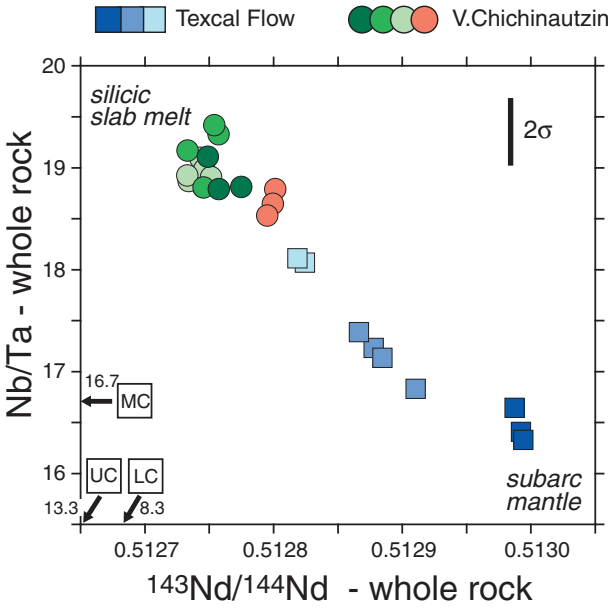

Fig. 11. Nb/Ta vs $^{143}Nd/^{144}Nd$ for the Texcal Flow and V. Chichinautzin volcanic rocks. Error bar indicates the 2σ of Nb/Ta based on repeat analyses. The inverse correlation argues against progressive assimilation of a low Nb/Ta crustal component by mantle melts. Nb/Ta ratios of upper (UC), middle (MC) and lower (LC) continental crust after Rudnick & Gao (2002).

basaltic mantle melt (≤49 wt % SiO_2, ≥10 wt % MgO), the proportion of the crustal material is fixed by mass balance (Fig. 10). Even in the most favorable case (highest possible SiO_2 of the crustal component), the Texcal Flow basalts would already contain ~10–30% of crustal material, whereas at V. Chichinautzin the proportion of the crustal contribution to the erupted melts increased to ~40–70%.

Such amounts of crustal material in the erupted melts, however, are unsupported by the other data. For example, the reversal of the Sr and Nd isotope trend at V. Chichinautzin (Fig. 5) argues against melt SiO_2 increase by increasing assimilation of ambient silicic crust into a common basaltic parental mantle melt. Moreover, even the most silicic V. Chichinautzin magmas have only weak arc signatures (Figs 3 and 4), which argues against significant uptake of strongly fractionated crustal components. Furthermore, the trends of some incompatible trace elements and their ratios with increasing melt SiO_2 are exactly opposite to the mixing trends formed by crust–mantle mixing. For example, Nb/Ta is high and inversely correlated with $^{143}Nd/^{144}Nd$, whereas crustal contamination should result in a trend towards low $^{143}Nd/^{144}Nd$ and Nb/Ta (Rudnick & Gao, 2002) (Fig. 11).

The strongest argument, however, against melt silica increase by crustal contamination is the high $^3He/^4He = 7–8$ R_a values of the olivines (Straub *et al.*, 2011*a*), which are similar to those of MORB-type mantle (8 ± 1 R_a; e.g. Farley & Neroda, 1998) (Fig. 12). Within the analytical error of ± 1 R_a, $^3He/^4He$ is indifferent towards bulk-rock

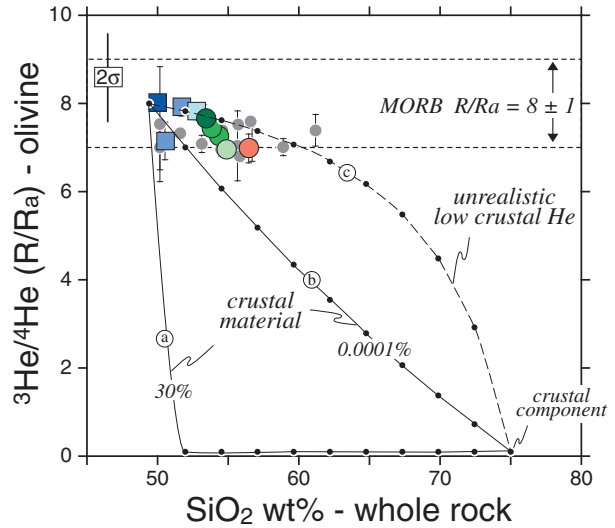

Fig. 12. Bulk-rock SiO_2 (wt %) vs air-normalized $^3He/^4He$ of olivine separates for the Texcal Flow and V. Chichinautzin. Grey filled circles are data for other central MVB volcanic rocks (Straub *et al.*, 2011*a*). External precision (2σ) of $^3He/^4He$ Ra is ± 1. Run error is within the symbol size unless indicated. MORB range after Farley & Neroda (1998). Mixing trends are calculated with the parameters listed in Table 2. Dots on curves denote 10% mixing intervals. Percentages on mixing curves a and b indicate the percentage of crustal material in the mantle melt. Curve c is unrealistic as it requires the crustal component to have only ~10–20% of the He of the mantle melt, which is not borne out by any known data (Ballentine & Burnard, 2002).

SiO_2, and the olivines from the basaltic Texcal Flow ($=7{\cdot}4+0{\cdot}4\,R/R_a$; $n=4$) are indistinguishable from those in the basaltic andesites of V. Chichinautzin ($=7{\cdot}3+0{\cdot}3\,R/R_a$, $n=4$). Such high $^3He/^4He$ values for the olivines, which represent the bulk-rock (Fig. 8), are inconsistent with the high sensitivity of U- and Th-depleted mantle melts towards the He-rich continental crust that has low $^3He/^4He$ ($<0{\cdot}1\ R_a$) from the ingrowth of radiogenic ^4He from crustal U and Th (O'Nions & Oxburgh, 1988; Martelli *et al.*, 2008).

The sensitivity to crustal contamination of mantle melts is supported by model trends (Fig. 12). The He abundances of mantle and crustal materials are difficult to constrain, but some reasonable assumptions can be made. We assume mantle He to be similar to the $He=1{\cdot}5\times10^{-5}\,cm^3\,STP\,g^{-1}$ in the MORB source (Allègre *et al.*, 1986–1987; Sarda & Graham, 1990). This maximizes mantle He, because OIB sources have less He ($1{\cdot}1\times10^{-10}\,cm^3\,STP\,g^{-1}$) (Moreira & Sarda, 2000). A 5% mantle melt then has $He=3{\cdot}0\times10^{-4}\,cm^3\,STP\,g^{-1}$, assuming perfect incompatibility of He during melting. The ^4He of the crustal component was estimated from $U=0{\cdot}568$ ppm and $Th=2{\cdot}61$ ppm, which is the average of upper and lower crustal xenoliths from within and around the MVB (Ruiz *et al.*, 1988; Roberts & Ruiz, 1989; Schaaf *et al.*, 1994; Lawlor *et al.*, 1999; Gómez-Tuena *et al.*, 2003; Martinez-Serrano *et al.*, 2004). The ^3He abundance of the crust is considered negligible. We calculated the abundance of radiogenic ^4He produced per year (minimum lifetime of the volcanoes) in a volume equal to the eruptive volume of the Texcal Flow and V. Chichinautzin ($\sim1\,km^3$, Siebe *et al.*, 2004*b*). Modeling parameters are given in Table 2. With these constraints, the Texcal Flow and V. Chichinautzin magmas would not tolerate even as little as 0·0001% of such crustal material (curve b) without the $^3He/^4He$ falling below the MORB range. In other words, a volume of $1\,km^3$ of mantle melt would tolerate $<3\,m^3$ of crustal material, which is far too low to cause a noticeable impact on melt SiO_2 and other major elements.

Importantly, the central MVB olivines mostly crystallize at pressures below 800 MPa, or <20 km crustal depth (Cervantes & Wallace, 2003; Roberge *et al.*, 2009). Thus, the high $He/^4He$ excludes assimilation in the lower crust. It could still be that the magma adsorbed upper crustal ^4He after crystallization of the olivines ('matrix contamination'; e.g. Stuart *et al.*, 2000). However, there is nothing in the isotope and trace element data that supports matrix contamination. For example, Sr and Nd isotopes, both sensitive to crustal contamination, form a tight array (Fig. 13) that contrasts strongly with the variable $^{87}Sr/^{86}Sr$ and $^{143}Nd/^{144}Nd$ of the ambient crust. However, the deviations from the mantle field are consistent with, and better explained by, additions of a homogeneous component rich in crustal Sr and Nd recycled from the slab. This is supported by the Pb isotope compositions of central MVB magmas, which are consistent with a strong slab signal (Gómez-Tuena *et al.*, 2003, 2007a; LaGatta, 2003; Martinez-Serrano *et al.*, 2004; Schaaf *et al.*, 2005). In summary, the high $^3He/^4He$ ratios of the olivines, in combination with all the other data, rule out crustal contamination as a cause of melt SiO_2 increase.

Silicic mantle melts by melt-rock reaction processes

Outline of a genetic model for the Texcal Flow and V. Chichinautzin

If crustal processing does not increase melt SiO_2, the high melt SiO_2 must be a characteristic of the initial mantle melts. Building on the high-Ni olivines, Straub *et al.* (2011*a*) proposed that basaltic and dacitic initial high-Mg# (>70) melts formed in the MVB subarc mantle by preferential melting of segregations of silica-deficient and silica-excess 'reaction pyroxenites' contained in a peridotite matrix. Melt mixing during ascent then produced hybrid basaltic andesitic and andesitic high-Mg# melts, which

Table 2: Parameters for mixing curves in Fig. 12

	SiO_2	$^3He/^4He$ R_a	He abundances (cm^3 STP g^{-1})		
	(wt %)		Curve a	Curve b	Curve c
Mantle melt[1]	49·0	8·0	3×10^{-4}	3×10^{-4}	3×10^{-4}
Crustal component[2]	75·0	0·1	$1{\cdot}16\times10^{2}$	$3{\cdot}87\times10^{-4}$	$3{\cdot}0\times10^{-5}$

[1]He abundance in mantle melt is equivalent to 5% melt from MORB source with $He=1{\cdot}5\times10^{-5}$ cm^3 STP g^{-1} (Allègre *et al.*, 1986–1987; Sarda & Graham, 1990) and assuming perfect incompatibility of He during melting.
[2]Crustal component calculated with $U=0{\cdot}568$ ppm and $Th=2{\cdot}61$ ppm from MVB crustal xenoliths (see text for data sources). Curve a: crustal end member has He equivalent to 30% of erupted magma volume of $1\,km^3$; curve b: crustal end member has He equivalent to 0·0001% of erupted magma volume of $1\,km^3$; curve c: assuming crustal component contains only 10% of He of the mantle melt (unrealistic).

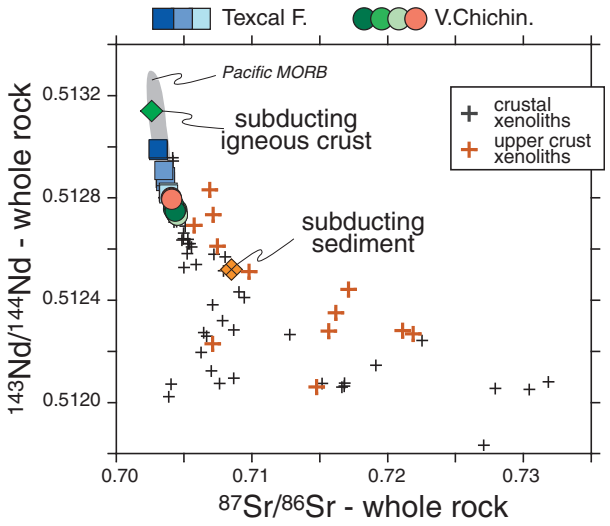

Fig. 13. $^{87}Sr/^{86}S$ vs $^{143}Nd/^{144}Nd$ for the Texcal Flow and V. Chichinautzin. Pacific MORB are zero-age data from mid-ocean ridge (GeoROC, 2011). Crustal xenoliths from within the MVB and adjacent basement outcrops (Ruiz *et al.*, 1988; Roberts & Ruiz, 1989; Schaaf *et al.*, 1994; Lawlor *et al.*, 1999; Gómez-Tuena *et al.*, 2003; Martinez-Serrano *et al.*, 2004). Subducting igneous crust and sediment after LaGatta (2003) and Gómez-Tuena *et al.*, (2007a).

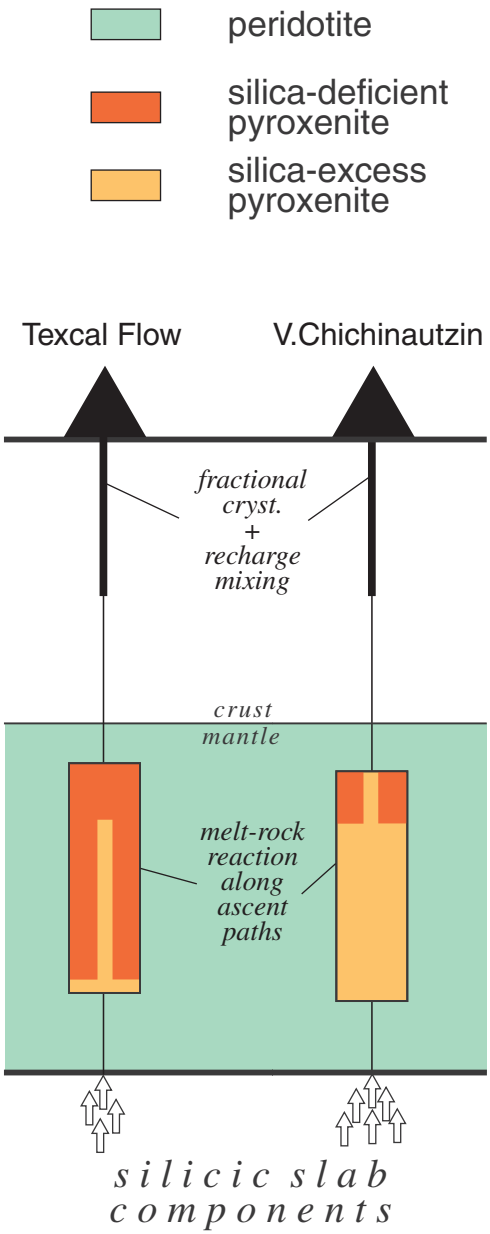

Fig. 14. Schematic illustration of Texcal Flow and V. Chichinautzin magma genesis. Genetic model is adapted from Straub *et al.* (2011*a*).

evolve at crustal depths to the low-Mg# magmas erupted by minor to moderate fractionation of mafic silicates (olivine, and possibly pyroxenes) and late-stage recharge mixing (Fig. 7b). This 'pyroxenite model' provides a genetic framework for melt evolution at Texcal Flow and V. Chichinautzin.

A schematic illustration of the model is given in Fig. 14. We propose that silica-deficient and silica-excess 'reaction pyroxenites' coexist in the mantle source of both volcanoes, whereby the silica-deficient pyroxenite overlies the silica-excess pyroxenite. Such 'stacking' can be seen as a consequence of the successive addition of silicic components from the slab. Initially, only sufficient slab SiO_2 is added to produce silica-deficient pyroxenites along the infiltration path. Re-use of this ascent path by later released silicic slab components (Hall & Kincaid, 2001) will gradually transform the lower part of the silica-deficient pyroxenite into silica-excess pyroxenite, whereby the pre-existing 'plug' of silica-deficient pyroxenite may prevent further reactive ascent of the slab components into the mantle wedge.

We propose that the time-progressive melt SiO_2 increase at Texcal Flow and V. Chichinautzin reflects sequential melting of such a zoned pyroxenite from top to bottom. In principle, the process is comparable with the draining of a stratified magma chamber that produces inversely zoned ignimbrites, with the key difference that Texcal Flow and V. Chichinautzin magmas progressively drain a mantle, and not a crustal magma reservoir. First, melts from silica-deficient pyroxenites dominate and basaltic melts erupt that may contain component melts from the surrounding peridotite. With time, continued melting increasingly integrates high-silica dacitic melts from the deeper, silica-excess pyroxenite, and the ascending hybrid magmas gradually become more andesitic.

The melts from the silica-deficient pyroxenite are best represented by the Texcal Flow magmas, which lack normative quartz (Fig. 15) and even have minimal normative nepheline in the earliest magmas (Table 1). In contrast, melts from silica-excess pyroxenite dominate at V. Chichinautzin. Texcal Flow and V. Chichinautzin erupt

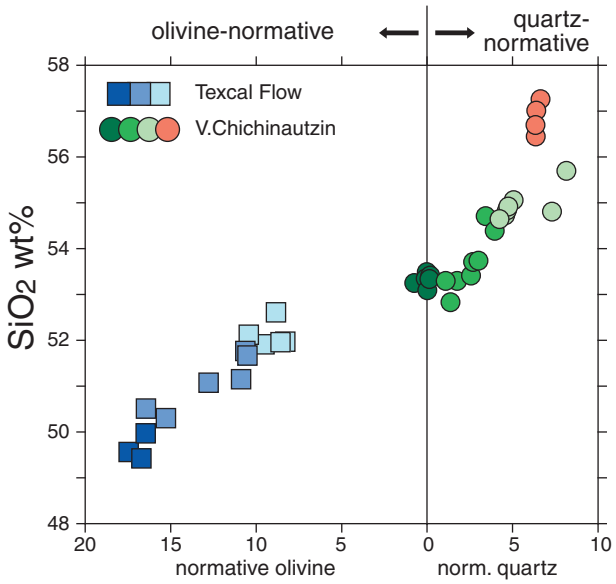

Fig. 15. Variation of normative olivine and quartz in the Texcal Flow and V. Chichinautzin volcanic rocks as a function of wt % SiO_2. CIPW norm calculation was performed with a program created by K. Hollocher at the Union College of Schenectady (http://www.union.edu/PUBLIC/GEODEPT/COURSES/petrology/norms.htm), with 18% ferric iron in total Fe.

either quartz- or olivine-normative magmas, except for some of the oldest distal lavas of V. Chichinautzin, which contain traces of normative olivine. Possibly, olivine-normative magmas may have erupted in the earliest stages of V. Chichinautzin and are now completely buried under the younger eruptive rocks. Despite this apparent separation, both volcanoes exhibit a range in melt SiO_2. This range can be explained only if partial melts from silica-excess and silica-deficient pyroxenites coexist in the region of melt formation, whereby the bulk composition of the erupted integrated melt (quartz- vs olivine-normative) must reflect the relative proportions of dacitic and basaltic initial melts contributing to the ascending hybrid melt.

Testing the pyroxenite model in trace element and isotope space

Below we discuss the variations in incompatible trace elements and $^{87}Sr/^{86}Sr$ and $^{143}Nd/^{144}Nd$ in the context of this model. The pyroxenite model implies that the mantle source of the Texcal Flow and V. Chichinautzin contains a significant amount of slab material. The proportion of slab material is constrained by the minimum amount of slab-derived SiO_2 needed to transform mantle olivine to 'reaction orthopyroxene'. This amount is fixed by the stochiometric reaction $SiO_2 + (Mg, Fe)_2SiO_4 = (Mg, Fe)_2Si_2O_6$. Assuming a background mantle of ~50–60% olivine, the resulting reaction pyroxenite (~50–60% reaction orthopyroxene, plus the original mantle ortho- and clinopyroxene) contains at least ~15–18% slab material. The percentage may increase as silica-excess pyroxenite forms, but may be lowered by integration of basaltic melts from the ambient peridotite. However, if only ~30% of the erupted melt mass originated from pyroxenite (and the rest from peridotite), the slab contribution in the magma would still be ~5–6%. Are these percentages consistent with the trace element patterns, and especially with the lack of a garnet signature in the Texcal Flow and V. Chichinautzin magmas?

Trace element variations

At first sight, the nearly flat patterns of incompatible trace elements (Fig. 3) suggest only very minor additions of slab fluids rich in Li, Pb, Rb and K to an enriched background mantle (e.g. Schaaf *et al.*, 2005). On the other hand, slab partial melts also transfer 'melt-mobile' elements [Th, Nb, Ta, Zr, Hf, light REE (LREE)] and thus blend with the sub-arc mantle in ways such that larger slab contributions are effectively concealed (e.g. Straub & Zellmer, 2012).

To test the latter possibility, we performed model calculations with REE and Y. These elements are melt-mobile, span a wide range of incompatible to moderately incompatible elements, and are sensitive to residual garnet. Moreover, their coherent behavior in petrogenetic processes balances to some extent the uncertainties inherent in the recycling modeling that involves many poorly known variables, such as the composition and residual phases of the subducted slab at arc front depths, the amounts of fluids and melts produced, as well as the partitioning behavior of single elements, which varies strongly with pressure, temperature and composition (e.g. Kessel *et al.*, 2005; Klimm *et al.*, 2008; Skora & Blundy, 2010). Thus, rather than deriving exact numbers, the modeling tests whether the REE and Y of the erupted magmas are compatible with the magnitude of the slab contributions implied by the reaction model. Modeling parameters are compiled in Table 3 and Electronic Appendix Table 3. Results are shown in Fig. 16.

The models first calculate the REE and Y contents of partial slab melts from the subducted sediment and basaltic igneous crust, respectively. A composite of the two slab melts is then added to the 'background mantle' (which is the subarc mantle prior to subduction modification). Then, partial melts of this metasomatized mantle are calculated, assuming solid source transformation to pyroxenite prior to melting. Figure 16 compares the modeled melts with four target compositions for the least and most silicic magmas from Texcal Flow and V. Chichinautzin. Modeling and results can be summarized as follows.

(1) Slab compositions are the terrigenous trench sediment from LaGatta (2003) and N-type MORB from Sun & McDonough (1989). The slab partial melts were calculated with the batch melting equation of Langmuir

Table 3: Summary of trace element modeling

Sample no.:		MCH06-12	CH05-16	CH08-5	S1
Volcano:		Texcal Flow	Texcal Flow	V. Chichinautzin	V. Chichinautzin
Eruptive unit:		Old Texcal Flow	Cuescomates vent	Distal lava flow	Summit lava
Background mantle (mantle without subduction components):		Primitive mantle (McDonough & Sun, 1995)	Primitive mantle (McDonough & Sun, 1995)	Primitive mantle (McDonough & Sun, 1995)	Residual mantle of McDonough & Sun (1995) after extraction of 7% melt
Modal composition of metasomatized mantle (%)	GRT	0·0	0·0	0·0	0·0
	OLIV	39	5	5	10
	OPX	46	85	85	87
	CPX	15	10	10	3
Ratio of sediment:igneous crust in composite slab component		30:70	30:70	50:50	50:50
Composite slab component in metasomatized mantle (%)		8	25	15	15
Extent of melting of metasomatized mantle (%)		5	5	3	3
Least-squares fit[1]		0·48	0·77	0·93	0·7
Elements added from slab (%)	La	35	68	63	95
	Ce	31	63	58	88
	Nd	23	53	46	72
	Sm	16	42	34	54
	Eu	11	33	24	39
	Y	2	7	4	7
	Yb	1	2	1	2
	Lu	0	2	1	1

Other reservoir compositions and partition coefficients are given in Electronic Appendix Table 3.
[1]The least-squares fit assesses the fit between model and measured composition. For each element, the value of x was calculated as follows: $x = [(\text{measured value} - \text{modeled value})/10\% \text{ of measured value}]^2$. If the average of x for all elements was <1, the fit was considered satisfactory.

et al. (1992) and the experimentally determined bulk partition coefficents (D) of Skora & Blundy (2010) (sediment) and Klimm *et al.* (2008) (basaltic igneous crust). These D values are for the elements La, Ce, Nd, Sm, Eu, Y, Yb and Lu, which have the advantage of having been determined in the same laboratory by similar techniques. In all models, the D values were kept constant, and the extent of slab melting was always an arbitrary 5%. The composite slab component contains between 30 and 50% sediment melt. As expected, the single and composite slab components display strong garnet signatures, with HREE and Y being up to a magnitude lower than for background mantle.

(2) The pyrolite of McDonough & Sun (1995) was taken to represent the background mantle beneath Texcal Flow and V. Chichinautzin. This choice is based on the fact that an ~3–5% partial melt of pyrolite closely resembles the old Texcal Flow, which is least affected by slab contributions (highest $^{143}Nd/^{144}Nd$, lowest $^{87}Sr/^{86}Sr$, least fractionated incompatible elements and lowest olivine Ni). Partition coefficients for mantle melting are from Donnelly *et al.* (2004). For the young summit lavas of V. Chichinautzin, partial depletion of the background mantle was assumed by previous extraction of a 7% melt, to simulate progressive mantle depletion by serial melting beneath a single volcano.

(3) Between 8 and 30% of the composite slab component was added to the background mantle. In all cases, the HREE of the background mantle dominate over any HREE added from the slab. Thus, the garnet signature of the slab melts vanishes, and the flat HREE patterns of the arc magmas are well reproduced. The

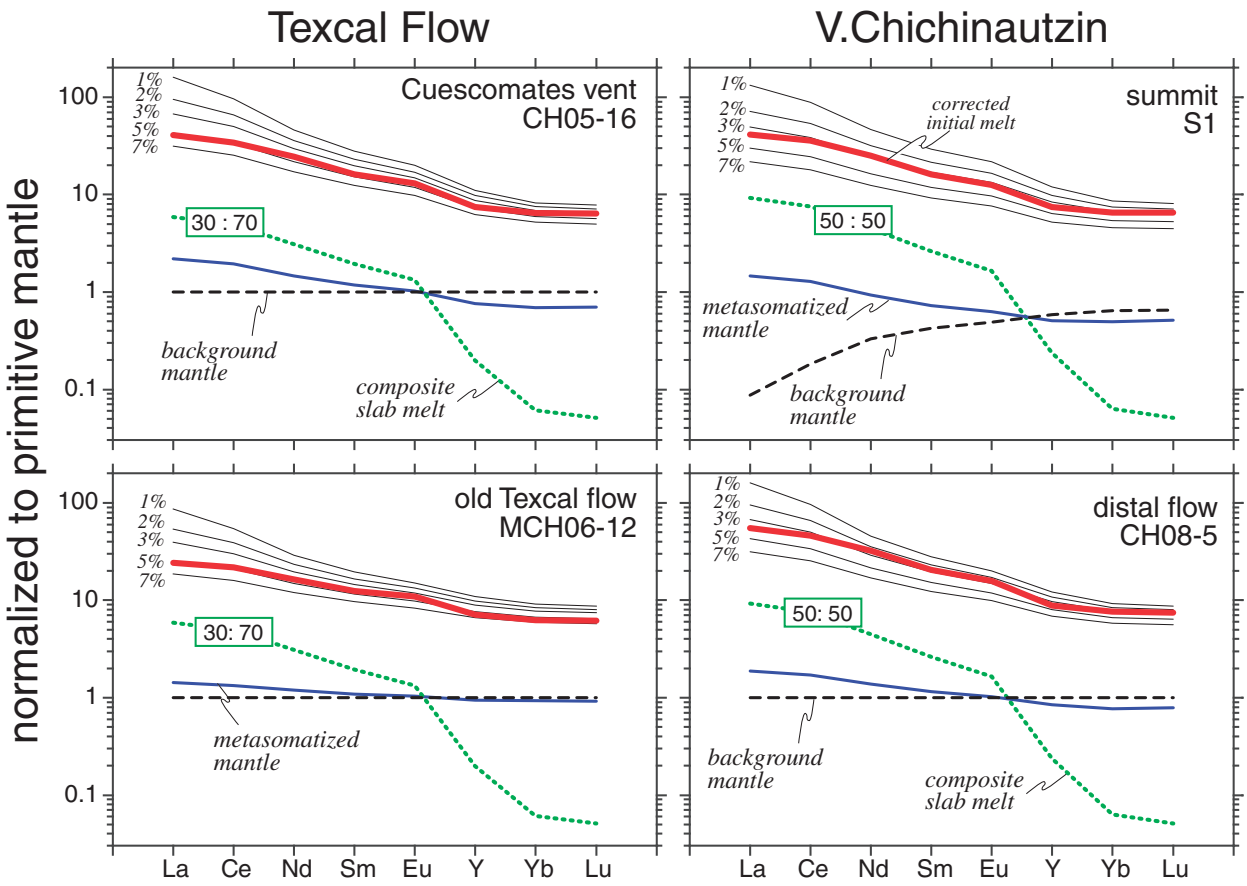

Fig. 16. Model calculations of REE and Y in selected samples of the Texcal Flow and V. Chichinautzin volcanic rocks. Data normalized to primitive mantle of McDonough & Sun (1995). Bold line (upper half of panels) indicates fractionation-corrected sample composition (to equilibrium with Fo_{88}); fine lines (upper half of panels), forward models for 1%, 2%, 3%, 5% and 7% extent of melting; dotted line, composite slab component of melts from subducted sediment melt and igneous crust, with the mixing ratio displayed in box; dashed line, background mantle; continuous line, metasomatized mantle (i.e. background mantle plus slab component). Modeling and input parameters are given in Table 3 and Electronic Appendix Table 3. (For discussion see text.)

slab contributions, however, increase the LREE of the magmas, up to a point where the slab flux of LREE controls arc chemistry and especially so if the mantle was previously depleted by melting.

(4) Melting of metasomatized mantle was simulated by a batch melting model with partition coefficients from Donnelly *et al.* (2004). Residual phases are olivine, orthopyroxene and clinopyroxene, but no residual garnet was needed. As in the reaction model, the proportions of olivine and orthopyroxene were varied in the model, but there is no perceptible effect on the REE and Y contents of the melts because the mineral and melt partition coefficients for olivine and orthopyroxene are very similar. The agreement of the model with the 'target compositions' (which are the erupted magmas corrected for fractionation to Fo_{88}) was tested by a least-squares fit (Table 3). The successful models shown in Fig. 16 require an extent of melting between 3 and 5%. However, larger extents of melting (up to 8%) are permissible, dependent on the choice of bulk D values and on the ratio of sediment to igneous crust in the composite slab component.

LREE mobility implies that other highly incompatible, melt-mobile elements, such as Nb, Ta, Zr and Hf, may also be transferred from the slab in significant amounts. For example, rutile-bearing eclogites may produce Nb-rich slab melts with high Nb/Ta (Stolz *et al.*, 1996; Klemme *et al.*, 2005; Gómez-Tuena *et al.*, 2011) and account for the increasing Nb/Ta with decreasing $^{143}Nd/^{144}Nd$ in the melt (Fig. 11). There are also slab controls on Zr and Hf in arc magmas (Gómez-Tuena *et al.*, 2011). Thus, the flat trace element patterns in the Texcal Flow and V. Chichinautzin volcanic rocks do not contradict the presence of substantial amounts of slab melt in the source. Given the complex behavior of recycled elements during prograde slab metamorphism (Gómez-Tuena *et al.*,

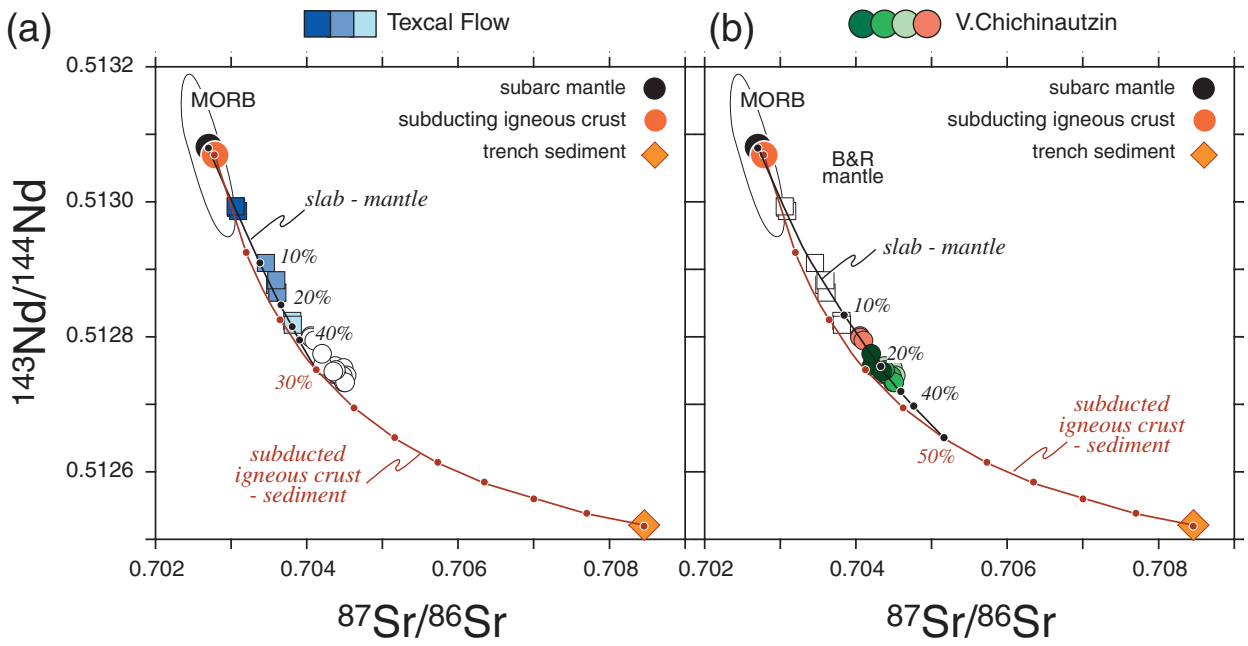

Fig. 17. $^{87}Sr/^{86}Sr$ vs $^{143}Nd/^{144}Nd$ mixing models for the Texcal Flow (a) and V. Chichinautzin (b) volcanic rocks. Zero-age MORB from the East Pacific Rise from PetDB (2011). Subducting igneous oceanic crust and sediment from LaGatta (2003) and Gómez-Tuena *et al.* (2007a). (For modeling parameters see Table 4; for discussion see text.)

2011) and serial mantle melting (Straub *et al.*, 2008), we limit further quantification to elements associated with isotopes.

Sr and Nd isotope variations

In $^{87}Sr/^{86}Sr$ vs $^{143}Nd/^{144}Nd$ space, the Texcal Flow and V. Chichinautzin volcanic rocks follow a tight continuous trend (Fig. 13). This trend can be reproduced by a three-component mixing model with background mantle and subducted igneous crust (both with high $^{143}Nd/^{144}Nd$ and low $^{87}Sr/^{86}Sr$), and trench sediment (low $^{143}Nd/^{144}Nd$ and high $^{87}Sr/^{86}Sr$), following the same mixing steps as in the trace element model. Results are shown in Fig. 17 and modeling parameters are summarized in Table 4.

If the Sr/Nd values of the slab components are retained, the calculated trends are concave, but still pass above the data (not shown). The data trend can be matched, however, assuming that Sr/Nd ratios change during slab processing and melt or fluid release from the slab, which may happen in various ways. For example, sedimentary Sr from a thin sediment layer may become lost during the flat, prolonged subduction beneath the MVB forearc (Savov *et al.*, 2005; Kim *et al.*, 2010). Alternatively, the flux of Sr from the igneous crust may increase gradually with increasing subduction depth relative to Nd that is retained in the slab (e.g. Kessel *et al.*, 2005). Also, the mantle may become impregnated by multiple 'fluid-like' and 'melt-like' slab components.

Closer inspection of the data reveals even more complexity. A single three-component mixing model can reproduce the isotope trends of both the Texcal Flow and V. Chichinautzin, but it fails to account for the large range in Sr/Nd. The Sr/Nd ~18–24 of Texcal Flow basalts is much higher than the Sr/Nd ~10–15 of V. Chichinautzin, as well as the Sr/Nd of the bulk slab components (trench sediment Sr/Nd ~7·0, igneous crust Sr/Nd ~12·3) and background mantle [Sr/Nd ~16; primitive mantle from McDonough & Sun (1995)]. As Sr and Nd are not fractionated during mantle melting, the range in Sr/Nd must be related to the slab flux. Intriguingly, the variable Sr/Nd in the magmas reflects principally the Nd variability by a factor of 2·5, whereas Sr remains nearly constant (factor of ~1·1) (Fig. 3). Thus, the slab flux of Sr (but not necessarily $^{87}Sr/^{86}Sr$) must be buffered, whereas the flux of Nd is variable. Figure 3 also shows that the old Texcal Flow has the lowest Nd, but displays the largest excess Sr relative to the mantle. Thus, the source of the old Texcal Flow appears to contain more Sr than Nd from the slab, possibly in the form of a fluid-like component rich in unradiogenic Sr from the igneous crust, but with negligible Nd. As the slab flux continues, the slab component may become more 'melt-like' and also entrain Nd, whereas the Sr content remains constant. This evolution continues until Nd contributions from the slab reach a maximum in the shield and cone magmas of V. Chichinautzin, and the slab flux to the source of the V. Chichinautzin summit magmas re-assumes more 'fluid-like' characteristics (lower Nd). Thus, rather

Table 4: Summary of Sr and Nd isotope modeling

	$^{87}Sr/^{86}Sr$	$^{143}Nd/^{144}Nd$	Nd	Sr	Sr/Nd
End member compositions					
Terrigenous trench sediment[1]	0·708460	0·512520	23·40	164·1	7·0
Subducting igneous crust[2]	0·702780	0·513070	7·30	90	12·3
Mantle wedge[3]	0·702700	0·513080	1·25	19·9	15·9
Texcal Flow model					
Mixing of subducted sediment and igneous crust					
Terrigenous trench sediment[4]	0·708460	0·512520	23·40	90[4]	3·8
Subducting igneous crust[5]	0·702780	0·513070	7·30	120[5]	16·4
Mixing of mantle and composite slab component					
Pre-impregnated mantle wedge[6]	0·702700	0·513080	1·15	29·9[6]	26·0
Composite slab component[7]	0·704162	0·512752	5[7]	111	22·2
V. Chichinautzin model					
Mixing of subducted sediment and igneous crust					
Terrigenous trench sediment[8]	0·708460	0·512520	23·40	130[8]	5·6
Subducting igneous crust[9]	0·702780	0·513070	7·30	180[9]	24·7
Mixing of mantle and composite slab component					
Mantle wedge	0·702700	0·513080	1·25	19·9	15·9
Composite slab component	0·704123	0·512752	12·13	155	12·8

[1]Terrigenous trench sediment from Deep Sea Drilling Project Site 467 after LaGatta *et al*. (2003).
[2]Isotope ratios estimated from average zero-age East Pacific Rise MORB (PetDB, 2011); Sr and Nd abundances are for average N-MORB after Sun & McDonough (1989).
[3]Isotope ratios based on mantle xenoliths from the Mexican Basin and Range Province (GeoROC, 2011); Sr and Nd abundances are for primitive mantle after Sun & McDonough (1989).
[4]Sr reduced by 45% in sediment, assuming early loss of Sr beneath forearc.
[5]Sr increased by 25% in igneous crust, assuming preferential release of Sr.
[6]Sr increased by 33% in mantle wedge, assuming pre-impregnation by Sr-rich fluid from igneous subducting crust.
[7]Nd reduced by 59% in composite slab components, assuming that Nd is retained in slab relative to Sr.
[8]Sr reduced by 21% in sediment, assuming early loss of Sr beneath forearc.
[9]Sr increased by 50% in igneous crust, assuming preferential release of Sr.

than being a single, homogeneous component, the slab flux continuously changes in its element abundance, and presumably also isotopic composition.

There is no single calculation for modeling evolving slab components with variable Nd abundances. Figure 17 depicts possible solutions for the Texcal Flow and V. Chichinautzin, respectively, that reproduce the observed $^{87}Sr/^{86}Sr$, $^{143}Nd/^{144}Nd$ and Sr/Nd by assuming the release of multiple slab components with variable Sr/Nd (Table 4). The model calculation does not take into account the variability of slab flux to either source, but focuses on reproducing the different Sr/Nd of each volcano. To reproduce the high Sr/Nd of the Texcal Flow, pre-impregnation of the Texcal mantle is assumed by a Sr-rich fluid from the igneous crust (Table 4). To this mantle, a composite slab component (mixture of sediment and igneous crust) is then added that has lost ~45% of the sedimentary Sr, but contains excess Sr (+ ~25%) from the igneous crust and retains preferentially Nd (up to ~59%). For V. Chichinautzin, satisfactory models are obtained with a composite slab component that has lost ~21% of the sedimentary Sr, but gained ~50% unradiogenic Sr from the igneous crust. Regardless of the problem of reproducing the Sr/Nd of the erupted magmas, all models require high amounts of slab-derived Sr and Nd in the arc magmas. Only the old Texcal Flow has fairly low amount of recycled Sr (~38% of the Sr in erupted arc magmas) and Nd (~31%). All the other Texcal Flow and V. Chichinautzin magmas would derive >50–84% of their Sr and Nd from the slab. Thus, the slab flux controls the Sr and Nd isotope chemistry of the arc magmas.

A control of arc Sr and Nd by the slab flux accounts for the relation of $^{87}Sr/^{86}Sr$ and $^{143}Nd/^{144}Nd$ with melt SiO_2 (Fig. 5). In this case, the variations in $^{87}Sr/^{86}Sr$ and $^{143}Nd/^{144}Nd$ with time should simply reflect the variable proportions of Sr and Nd contributed from subducted sedimentary and igneous crust. The trend at Texcal Flow would then reflect the increasing melt-like slab flux of

sedimentary Sr and Nd with time and continuing formation of silica-excess pyroxenite in the source. Although the beginning of this evolution is recorded at V. Chichinautzin, the later reversal in $^{87}Sr/^{86}Sr$ vs $^{143}Nd/^{144}Nd$ space may reflect the exhaustion of the flux of Sr and Nd from the thin sedimentary layer that subsides with time in favor of the fluid-like Sr and Nd flux from the much more voluminous igneous crust below. However, silica-excess pyroxenites (which will eventually convert to silica-rich partial melts) continue to build up in the source, regardless of the changing slab flux of Sr and Nd. In other words, the time-progressive trends at Texcal Flow and V. Chichinautzin record the release of a sediment-rich component from the slab that is set against the background of a continuous slab flux from the igneous crust.

Each volcano has at least three eruptive units with distinct $^{87}Sr/^{86}Sr$ and $^{143}Nd/^{144}Nd$. In the genetic model proposed, this would signify the multiple infiltration events of slab material that builds progressively the heterogeneous, zoned reaction pyroxenite. Possibly, more infiltration events occur that are not distinguishable in the isotopes. There is no information on the period over which pyroxenite segregations may form and how long they may reside in the mantle wedge prior to melting. It is conceivable that the reaction pyroxenites formed in the lower mantle wedge near the slab interface and became entrained into, and added to the buoyancy of, upwelling mantle. Once melting started, however, the pyroxenite segregations must be drained within the short life-time of monogenetic volcanoes, typically less than a few decades.

Alternative models

Other mechanisms have been proposed that may either increase melt SiO_2 or the Ni content of magmatic olivine. For example, the SiO_2 contents of partial melts of peridotite may increase by several wt % in the presence of water (e.g. Baker *et al.*, 1994; Hirose, 1997; Carmichael, 2002). Although OIB-type MVB magmas tend to be less hydrous than the calc-alkaline MVB volcanic rocks (up to 6 wt % H_2O; Cervantes & Wallace, 2003; Roberge *et al.*, 2009), they still contain ~2–3·2 wt % H_2O in the Sierra Chichinautzin Volcanic Field (Cervantes & Wallace, 2003a; Johnson *et al.*, 2009). Weber *et al.* (2011) have suggested that mantle olivine may become unusually Ni-rich through diffusive uptake of Ni from percolating sulfide melts, which would result in melts with high-Ni olivine. In another model, Matzen *et al.* (2012) proposed a temperature dependence of Kd_{Ni}^{oliv} that would increase the Ni content in magmatic olivine relative to the olivine in the mantle source. If such processes worked together in favorable ways, Ni-rich olivine could precipitate from hydrous, silicic melts.

However, there are problems. In particular, it is unclear how processes that are independent of each other can produce the coherent trends observed. There is no obvious reason why a temperature- or sulfide-driven Ni increase in magmatic olivine, hydrous melting and melt-like, Sr–Nd-bearing slab components should come together to form the observed temporal succession at Texcal Flow and V. Chichinautzin. Moreover, melt inclusion studies reveal no relation between melt H_2O and SiO_2 content, as olivine-hosted melt inclusions from basaltic MVB magmas have similar high H_2O to andesitic magmas (Cervantes & Wallace, 2003; Roberge *et al.*, 2009). Diffusive Ni enrichment by coexisting sulfide melts seems to be a spatially limited, micro-scale process that has been observed only in a single xenolith out of a whole suite (Ishimaru & Arai, 2008). The proposed temperature-dependent increase of the Kd_{Ni}^{oliv} is insufficient to explain the range of magmatic olivine compositionsin central Mexico, and may be less efficient in hydrous, silicic melts than in the anhydrous high-MgO picrites considered by Matzen *et al.* (2012). In contrast, the reaction pyroxenite model provides a plausible link between all these observations in time and space, and predicts a maximum Ni content for the magmatic olivines that agrees with the values observed (Straub *et al.*, 2008, 2011*a*).

Modification of silicic mantle melts in the overlying crust

The pyroxenite model predicts the formation of high-Mg# >70 (corresponding to $>Fo_{88}$) initial melts with basaltic to dacitic melt SiO_2 contents (Straub *et al.*, 2011*a*). Thus, the lower Mg# values of the erupted Texcal Flow and V. Chichinautzin magmas must be due to crustal processing, which is most probably associated with the fractionation of olivine, or possibly pyroxenes (Straub *et al.*, 2011*a*). This requirement underlines the importance of crustal processing of the initial Texcal Flow and V. Chichinautzin magmas.

Possibility of early pyroxene crystallization

At low to moderate melt H_2O contents (approximately <2–3 wt %), pyroxenes may be on the liquidus at lower crustal pressures (Weaver *et al.*, 2011; Weber *et al.*, 2011). In Fo–Ni space, the olivines of V. Chichinautzin display a gap of a few mol % Fo between the olivines observed (maximum Fo_{86}) and those presumed to be equilibrium with the initial mantle melts ($>Fo_{88}$) (Fig. 18). Although this gap can be bridged by only a few per cent of olivine fractionation, it may also signify early, cryptic pyroxene crystallization. Figure 18 depicts the possible trends of early ortho- and clinopyroxene fractionation in Fo–Ni space. Pyroxene loss does not much affect melt SiO_2, but lowers noticeably the melt Mg#, albeit at a lesser rate than olivine loss. Melt Ni decreases only slightly, as Ni is only moderately compatible in pyroxene (Beattie *et al.*, 1991). The gap for V. Chichinautzin olivines can be closed by a few per cent of orthopyroxene fractionation (~5–7%); however, clinopyroxene fractionation would

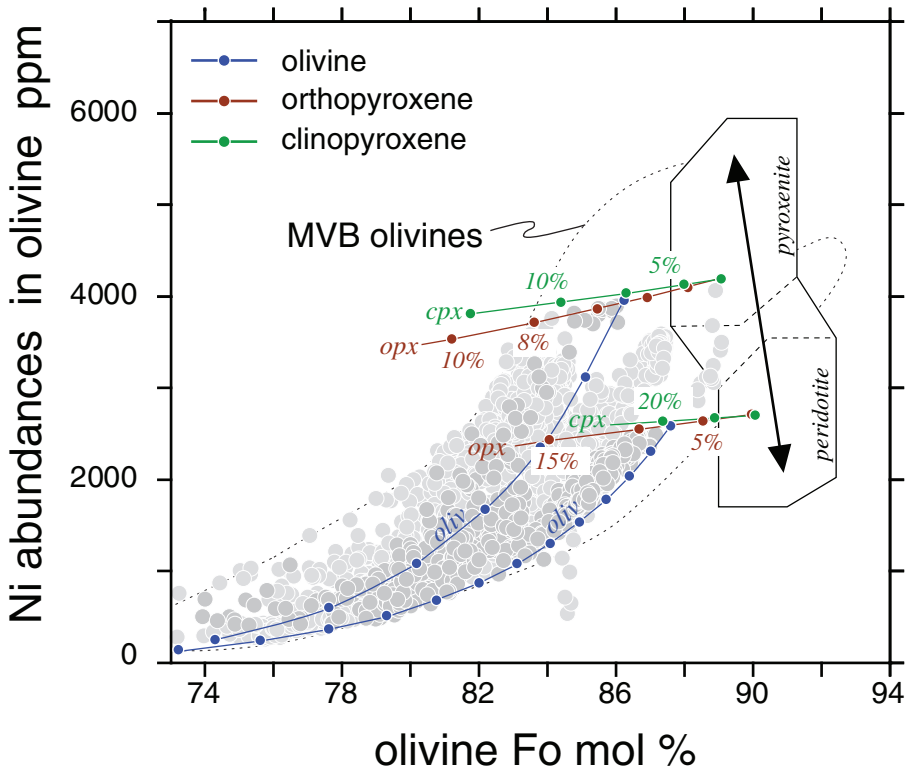

Fig. 18. Fo mol % vs Ni ppm for olivines in the Texcal Flow and V. Chichinautzin volcanic rocks. The variant of the genetic model in Fig. 7 depicts high-pressure fractionation of pyroxenes prior to olivine stabilization at shallow crustal levels. Starting melts are at 5·4 wt % MgO, 4·0 wt % FeO and 129 ppm Ni for high-Ni olivine and at 9 wt % MgO, 6 wt % FeO and 210 ppm Ni for low-Ni olivine. (See text for discussion.)

need to amount to ~10–20 wt %, depending on the FeO and MgO content of the initial hybrid melts. Clearly, early orthopyroxene crystallization is feasible and must be considered. On the other hand, there are no correlations of CaO or CaO/Al_2O_3 with Mg# in the various eruptive units that would support a role for early clinopyroxene crystallization. Overall, the more silicic, viscous V. Chichinautzin magmas seem more prone to early pyroxene fractionation than the less viscous, more mobile basaltic Texcal Flow magmas, which may pass more rapidly through the crust.

Crustal filtering and modification of initial melt signatures

Crustal processing also accounts for the higher melt Mg# values of the silicic young Texcal vent lavas. In the simplest way, this is the consequence of a smaller loss of mafic phases relative to the earlier Texcal magmas (Fig. 19). Variable fractionation of mafic phases can also cause the distal and shield lavas at V. Chichinautzin to have different Mg# values despite their similar SiO_2 contents. However, the mixing evidence preserved in the olivines suggests that the erupted bulk magmas are not simply derivative melts, but hybrids of two and more derivative melts that mixed after having experienced some olivine fractionation. Because the olivines had already crystallized (implying upper crustal depths), melt mixing most probably occurs by 'recharge mixing' involving mixing of existing and newly ascending magmas at upper crustal levels. Recharge mixing may be less efficient in the Texcal Flow where the olivines of the various eruptive units are largely separated in Fo–Ni space, which argues against interaction of the magmas from the different eruptive units (Fig. 20). However, at V. Chichinautzin the olivines overlap widely along the same broad mixing and crystallization trend (Fig. 21), which could be due, at least in part, to protracted recharge mixing with the silicic, viscous V. Chichinautzin magmas prior to eruption.

Is crustal processing efficient in erasing the signatures of initial mantle melts? With their high melt SiO_2 contents of ~57 wt %, the young summit lavas of V. Chichinautzin should best represent the silicic partial melts from silica-excess pyroxenites. On the other hand, these magmas already have low Mg# values and olivine Fo and Ni contents (despite high $^3He/^4He$) that are similar to those of olivines that would crystallize from partial melts of peridotite; only a few high-Ni olivines could be xenocrysts from earlier magmas. As such, the derivation of the V. Chichinautzin summit magmas from pyroxenites is substantially based on the interpretation of the earlier series, where the tell-tale high-Ni olivines are better preserved.

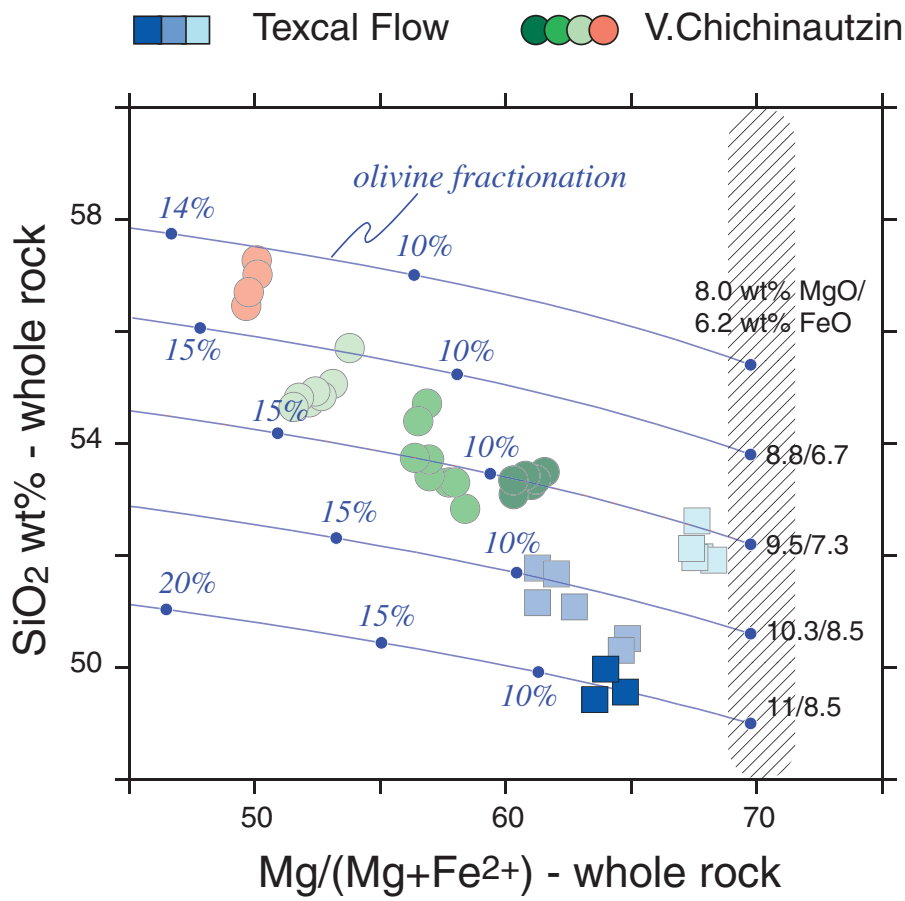

Fig. 19. Bulk-rock SiO_2 vs Mg# of the Texcal Flow and V. Chichinautzin. Continuous lines with dots are calculated olivine fractionation trends, with the percentage of olivine fractionation given in italics, and with the MgO and FeO* of the initial bulk melt indicated. Diagonally shaded field indicates the range of initial mantle melts after Straub *et al.* (2011*a*). The small effect on melt SiO_2 relative to the decrease in melt Mg# owing to the preferential uptake of MgO in olivine relative to FeO should be noted.

Clearly, this observation implies that a pyroxenite provenance may also be obscured in the low-Mg# andesites and dacites that prevail in other major Mexican composite volcanoes such as Nevado de Toluca or Volcan Popocatepetl.

The sources of major element oxides—mantle vs slab origin

The arc signature in Texcal Flow and V. Chichinautzin magmas

In major element space, the Texcal Flow and V. Chichinautzin magmas exhibit a clear arc affinity relative to MORB or the enriched basalts from the Mexican Basin and Range Province (B&R basalts), which have been suggested to represent the subarc MVB mantle prior to subduction modification (Fig. 2; Luhr, 1997; Gómez-Tuena *et al.*, 2003, 2007b, 2011; Blatter *et al.*, 2007; Johnson *et al.*, 2009). Key features are the enrichment in Na_2O and K_2O and the depletion in CaO in the Texcal Flow and V. Chichinautzin lavas (Plank & Langmuir, 1988), and higher SiO_2 and Al_2O_3 that are coupled with lower FeO, MgO and TiO_2 relative to the B&R basalts. The arc affinity is most obvious in SiO_2 vs Na_2O+K_2O space, where the Texcal Flow and V. Chichinautzin eruptive rocks define a tight trend outside the field of mantle magmas trending towards the MVB andesites (Fig. 22). Given the high percentages (~5–30%) of slab material in the mantle source, it may well be that other major elements than SiO_2 were also added from the slab in significant amounts, in particular Al_2O_3, K_2O and Na_2O, which are the principal components of alumino-silicate slab fluids (e.g. Beard & Lofgren, 1991; Rapp & Watson, 1995; Kessel *et al.*, 2008). On the other hand, oxides such as TiO_2 and P_2O_5 are well above the levels of arc magmas (e.g. Gill, 1981). Although their enrichment has been interpreted to signify a melt origin from enriched mantle sources (e.g. Wallace & Carmichael, 1999; Schaaf *et al.*, 2005; Blatter *et al.*, 2007), the pyroxenite model provides other possibilities.

Interpreting the major element oxides

Given the fractionation of only some olivine (and possibly orthopyroxene), the fractionation-corrected element

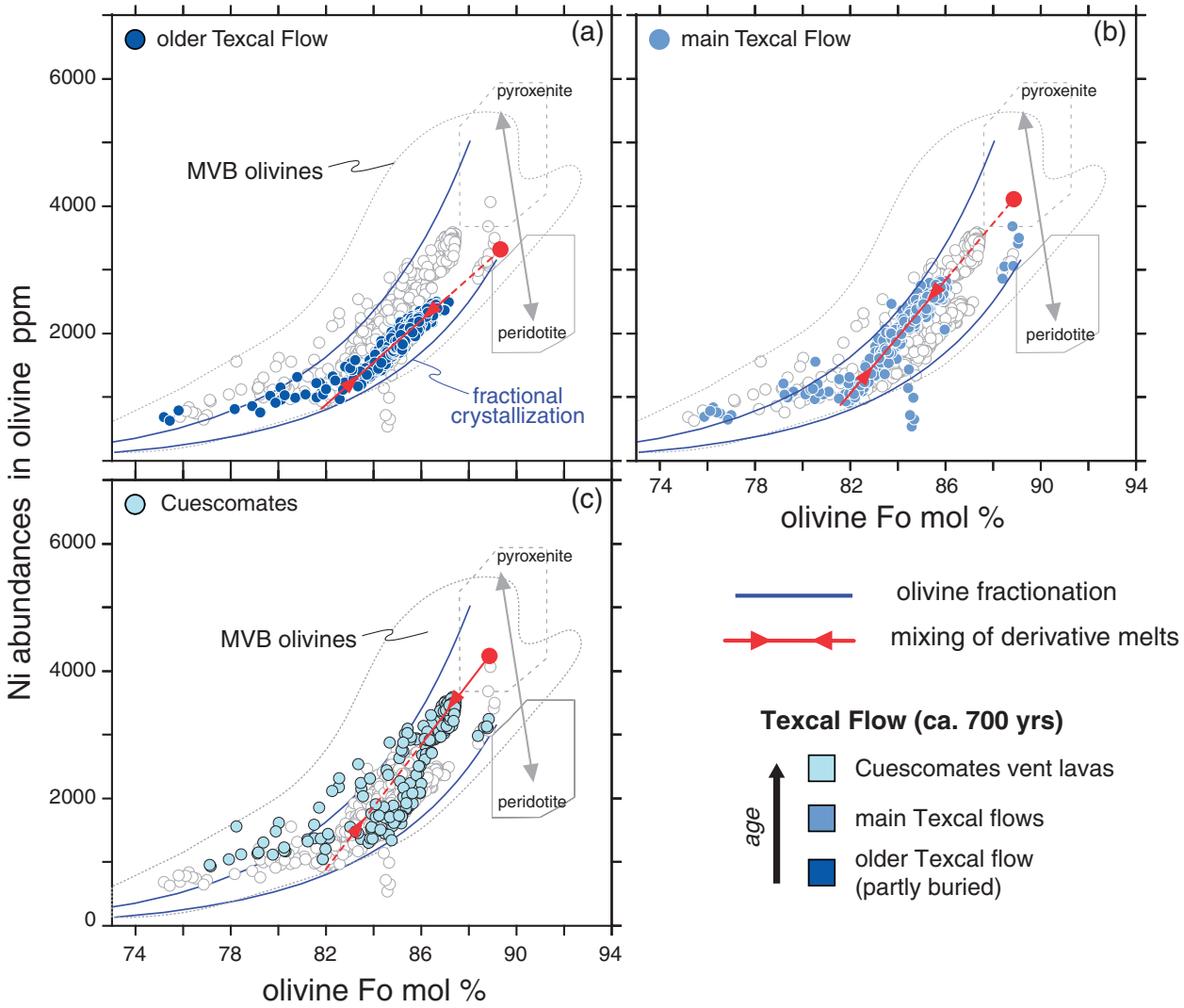

Fig. 20. Variation of Fo vs Ni in olivine from the different eruptive units of the Texcal Flow. (a) Old Texcal Flow; (b) main Texcal flow; (c) Cuescomates vent lavas. Only olivine cores are shown for clarity. Continuous lines are examples of calculated trends of fractional crystallization.

abundances shown in Fig. 9 must reflect the systematics of the initial mantle melts. Two groups can be distinguished. The first group shows inverse correlations with Si_{88}, either continuously or separated by an offset (e.g. Fe_{88} and Mg_{88}). In the context of the pyroxenite model, these correlations would reflect mixing between the basaltic and silicic mantle melts. Basaltic melts have low Si_{88} and high Ca_{88}, Fe_{88}, Mg_{88} and Ti_{88}, whereas silicic melts are rich in Si_{88}, but depleted in Ca_{88}, Fe_{88}, Mg_{88} and Ti_{88}. The lack of enrichment with Si_{88} further suggests that Ca, Fe, Mg and Ti in the Texcal Flow and V. Chichinautzin magmas were principally mantle-derived, in agreement with experimental data that show that these elements are not transported in silicic slab components (Beard & Lofgren, 1991; Johnson & Plank, 1999; Rapp *et al.*, 1999).

The second group of elements comprises Al_{88}, Na_{88}, K_{88} and P_{88}, which form no coherent correlations with Si_{88}. Importantly, no correlations occur among these elements that could be attributed to partial melting of a homogeneous mantle source, such as co-correlations of Ti_{88} with Nb_{88}, Na_{88}, P_{88} or K_{88}, all of which are incompatible during melting of peridotite or pyroxenite mantle (Fig. 23). At Texcal Flow, Ti_{88} correlates inversely with P_{88}, Nb_{88}, Na_{88} and K_{88}, which is opposite to predicted melting trends. At V. Chichinautzin, Ti_{88} co-correlates only with P_{88}, Nb_{88} and K_{88}, but not with Na_{88}. Moreover, the relative increase in K_{88} (11%) within the series is much less than the increases in Ti_{88} (28%), Nb_{88} and P_{88} (both 42%), whereas melting systematics predicts that K and Nb should be more strongly enriched than Ti and P. There

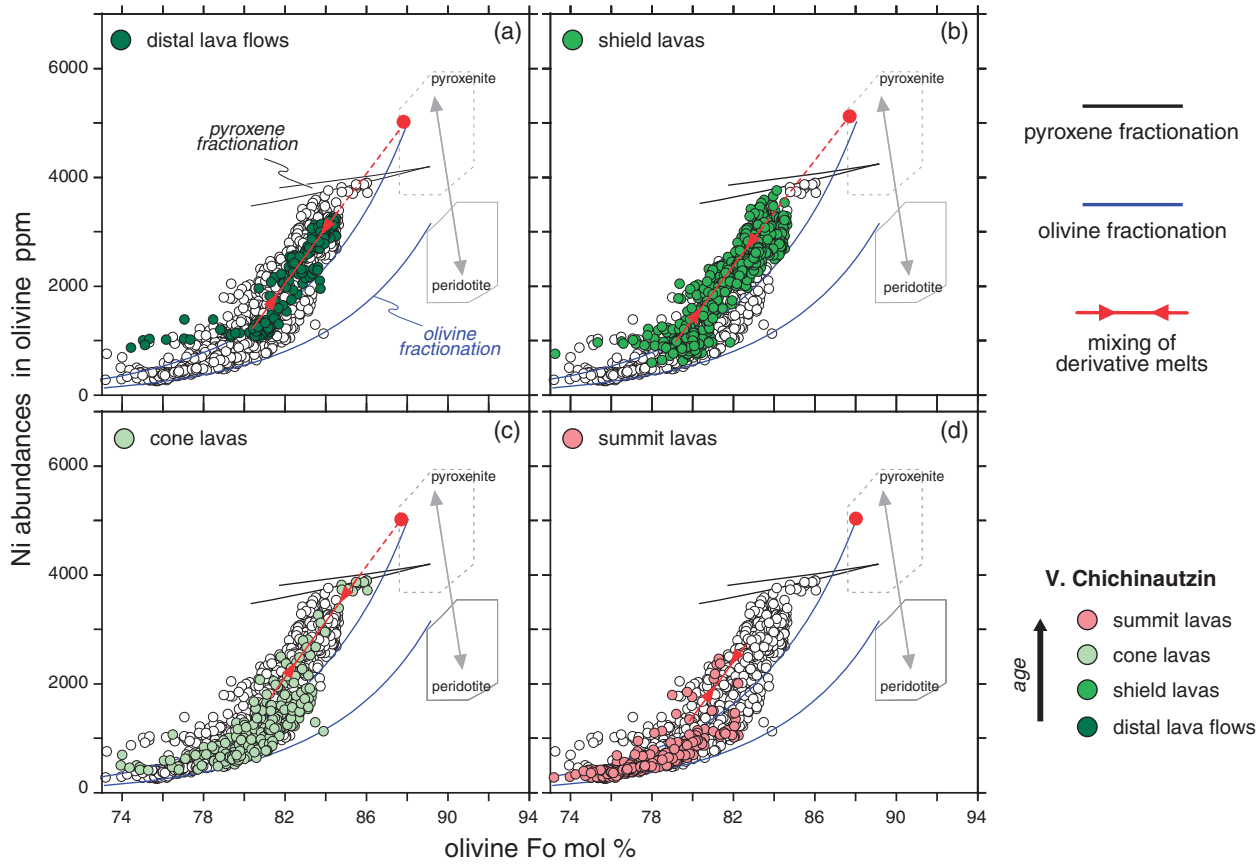

Fig. 21. Variation of Fo vs Ni in olivine from the different eruptive units of V. Chichinautzin. (a) Distal lavas; (b) shield lavas; (c) cone lavas; (d) summit lavas. Only olivine cores are shown for clarity. Continuous lines are examples of calculated trends of fractional crystallization. The possibility of early pyroxene fractionation is indicated. Overlap in olivines from different eruptive units, and the mostly low-Ni olivine in the silicic summit lavas should be noted.

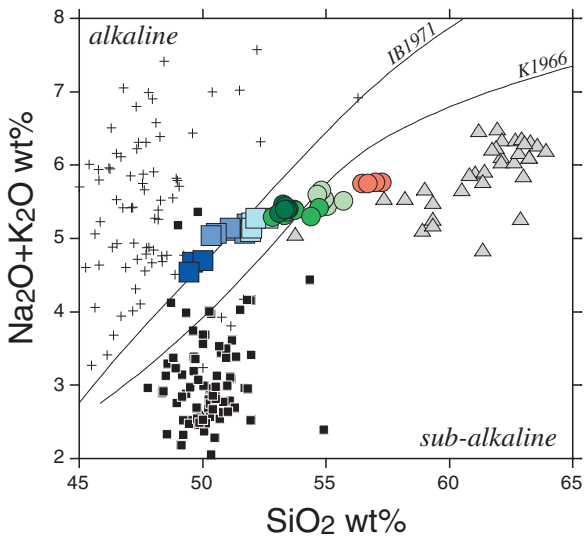

Fig. 22. Variation of SiO_2 vs total alkalis ($Na_2O + K_2O$) (in wt %). Dividing lines between alkaline and sub-alkaline fields after Irvine & Baragar (1971) (IB1971) and Kuno (1966) (K1966). The Texcal Flow and V. Chichinautzin volcanic rocks show a trend outside the field of mantle magmas towards the calc-alkaline andesites of Popocatepetl. Data sources and symbols as in Fig. 2.

is no evidence that residual phases in the mantle source may explain these inconsistencies. For example, the lack of correlation between Nb_{88} and Ti_{88} rules out rutile, whereas residual amphibole is unsupported by the incompatible trace elements as discussed above.

Thus, the mantle source of the Texcal Flow and V. Chichinautzin must be heterogeneous with respect to these elements. The co-correlation of Nb_{88}, K_{88} and P_{88} with Sr and Nd isotopes (shown for $^{143}Nd/^{144}Nd$ in Fig. 24) points to slab-induced metasomatism as the cause of source heterogeneity. The relationship between Na_{88} and $^{143}Nd/^{144}Nd$ is ambiguous. Na_{88} increases slightly with decreasing $^{143}Nd/^{144}Nd$ at the Texcal Flow, but the positive correlation at V. Chichinautzin seemingly argues against a slab origin. However, $Na_{88} = 3{\cdot}5–3{\cdot}9$ wt % barely varies relative to the much larger range of Nb_{88}, K_{88} and P_{88}. This may signify a constant, high slab flux of Na that was decoupled from the elements K, P and Nb. Lastly, Al_{88} does not co-correlate with K, P or Nb, nor with the Nd–Sr isotopes (not shown). The lack of correlation is not unexpected, because melt Al, like Si, is governed by other factors than incompatibility during melting. Thus, although

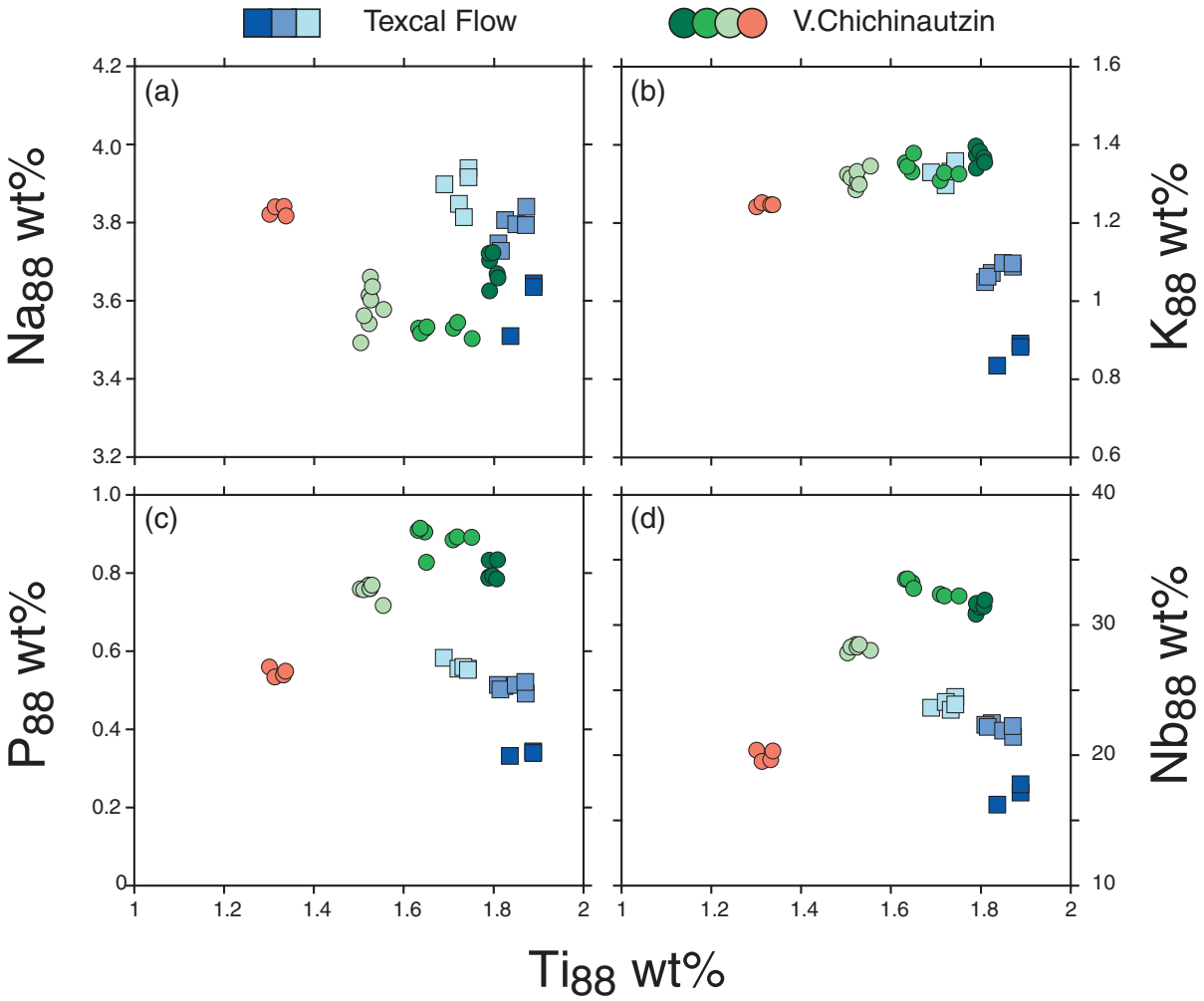

Fig. 23. Fractionation-corrected variations of Ti_{88} vs Na_{88} (a), K_{88} (b), P_{88} (c), and Nb_{88} (d). The relationships cannot be attributed to melting of a homogeneous mantle source, which would predict co-correlations of these incompatible elements.

Al is likely to be released from the slab to some extent, this effect is hard to detect in the erupted magmas.

In summary, we conclude that the major elements Si, K, Na, P and Nb (and possibly Al) were added in significant amounts from the slab to the mantle wedge. A slab addition of P and Nb implies that much of the apparently enriched 'OIB-type' signature of the Texcal Flow and V. Chichinautzin is due to subduction recycling, and does not reflect an inherently enriched subarc mantle.

Quantitative contribution and inferences on the composition of the subarc mantle

Quantifying the proportion of slab-derived major elements in arc melts is difficult. Nevertheless, we attempt an estimate using primitive mantle as the background mantle. This choice of background mantle is also supported by the moderately incompatible element Ti that should be principally sourced from the mantle. In this case, the abundance of Ti in the melt depends only on the source composition and extent of melting (F, fraction of melt produced). Forward modeling of various N-type MORB sources (McDonough & Sun, 1995; Donnelly *et al.*, 2004; Workman & Hart, 2005) shows that even at the lowest possible F values of a few per cent (Davis *et al.*, 2011), the high Ti_{88} of ~2 wt % cannot be produced. However, the Ti_{88} can be reproduced by very low extents of melting ($F = 1$–4%) of a primitive mantle source (Sun & McDonough, 1989; McDonough & Sun, 1995). Interestingly, even primitive mantle is too depleted in Ti to produce the B&R basalts, which have mostly $Ti_{88} > 2$ wt %. The lower Mg_{88} and Fe_{88} of the Texcal Flow and V. Chichinautzin relative to the B&R basalts preclude them from being related by different extents of melting. Thus, the Texcal Flow and V. Chichinautzin, and the B&R basalts cannot originate from the same mantle source.

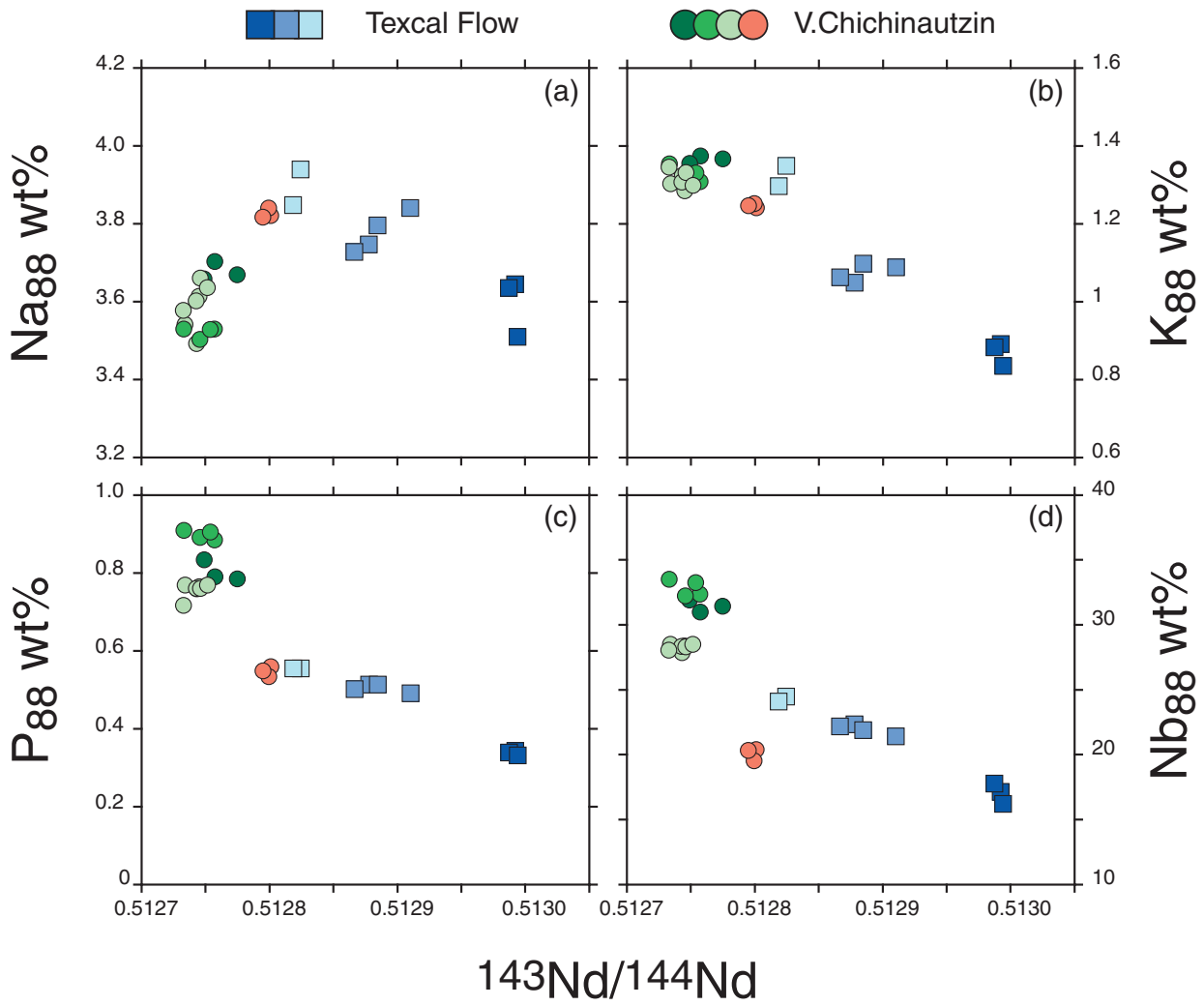

Fig. 24. Trends of $^{143}Nd/^{144}Nd$ vs fractionation-corrected abundances of Na_{88} (a), K_{88} (b), P_{88} (c), and Nb_{88} (d). The inverse correlations with K_{88}, P_{88} and Nb_{88} suggest that these elements are recycled in significant amounts from the slab.

K, Na and P all behave incompatibly during mantle melting. In this case, the difference in K, Na and P contents in melts from the background mantle compared with the abundances observed in the arc melt provides a measure of the leverage by the slab flux. K and Na are more incompatible in olivine than in orthopyroxene, and hence the peridotite–pyroxenite transformation will tend to minimize the slab signal. Assuming bulk distribution coefficients $D_K = 0{\cdot}025$, and $D_{Na} = 0{\cdot}5$ for melting, approximately 60% of the K_{88} and 82% of the Na_{88} in the erupted magmas would be recycled from the slab. Such a high slab flux agrees with the fairly high and constant melt abundances of K and Na, which favor a strong slab control on arc magma K and Na, rather than moderation through mantle melting processes.

It is more difficult to estimate the slab flux of P, because the K_{dP}^{oliv} ~0·1 is higher than the Kd_{dP}^{opx} ~0·03 (Brunet & Chazot, 2001). This enhances the 'slab signal' by ~30–40% for the same amount of P in the source, because melts from 'reaction pyroxenites' are more enriched in P than peridotite melts (Fig. 25, Table 5). Thus, the high P contents of Texcal Flow and V. Chichinautzin—and their similarity to OIB-type basalts—may also reflect the lithological transformation of the mantle source. However, despite the 'enhancement', P needs to be enriched by up to twice as much as in primitive mantle to match the Texcal Flow and V. Chichinautzin levels. This suggests P addition from the slab, and as much as ~17–50% of the P in Texcal Flow and V. Chichinautzin magmas may be slab-derived. If the slab flux of P varied with time, then the gooseneck curve in P_2O_5 vs Mg# space could form (Fig. 2), which is reminiscent of a fractional crystallization trend.

Silicon and aluminum are major elements in the mantle. Slab-derived SiO_2 triggers the reaction to form pyroxenite

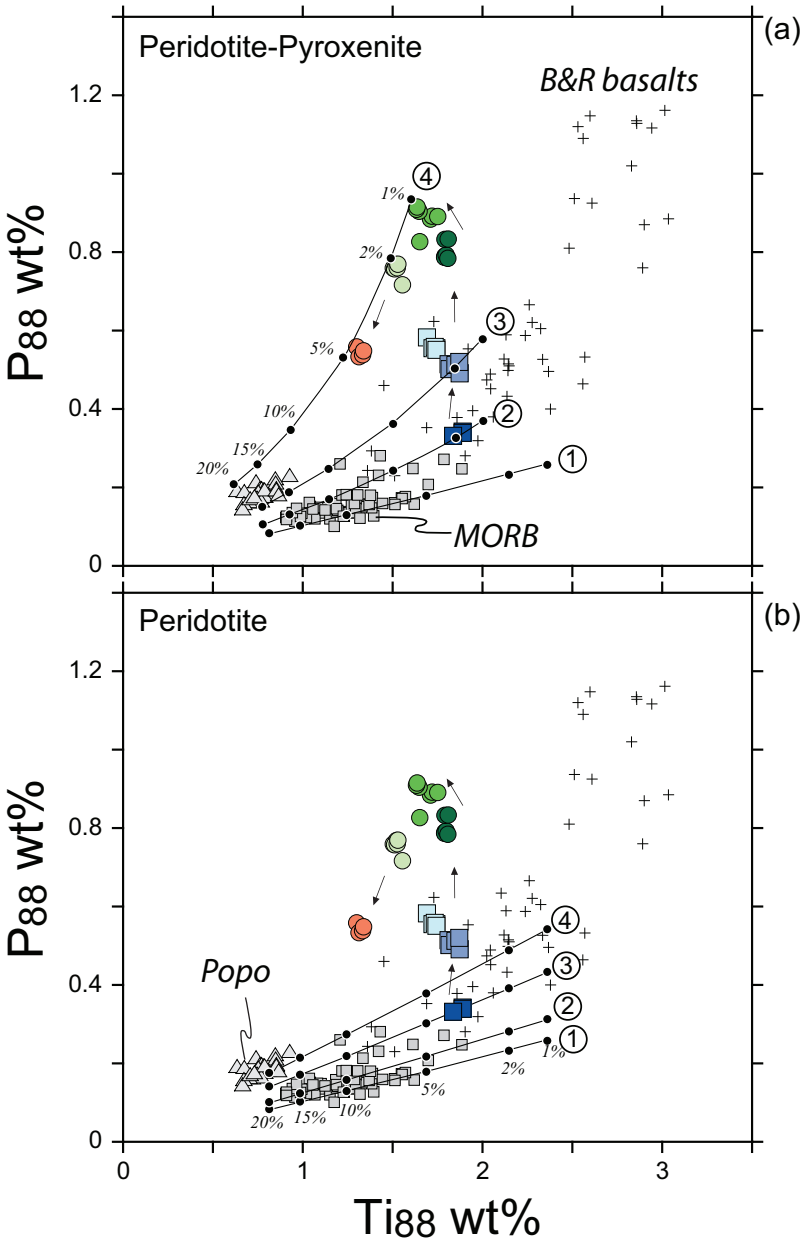

Fig. 25. Modeled trends of P_{88} vs Ti_{88} for mixed peridotite–pyroxenite (a) and peridotite (b) mantle source lithologies. Texcal Flow and V. Chichinautzin data are compared with Popocatepetl (grey triangles), MORB (grey squares) and B&R basalts (crosses). Mineral/melt partition coefficients are from Brunet & Chazot (2001) and Adam & Green (2006). Model parameters are given in Table 5. Source abundances of TiO_2 and P_2O_5 are the same for a given model curve (1–4) in either lithology. Phase proportions are kept constant in peridotite, but the percentage of orthopyroxene increases at the expense of olivine in the mixed peridotite–pyroxenite source (see Table 5). The difference of P_2O_5 in the model curves (continuous lines with dots) in (a) and (b) solely reflects the lower $K\mathrm{d}_P^{ol}$ relative to $K\mathrm{d}_P^{opx}$.

and hence—as outlined above—the erupted magmas may contain as much as 15–18 wt % of slab-derived SiO_2. Al_2O_3 is very probably entrained to some degree in the slab flux (e.g. Beard & Lofgren, 1991; Johnson & Plank, 1999; Kessel *et al.*, 2005); however, we attempt no quantitative estimate, given the sensitivity of melt Al_2O_3 to other factors (pressure, H_2O content, extent of melting) than source abundances during mantle melting.

In summary, we propose that the abundance of major element oxides in the Texcal Flow and V. Chichinautzin magmas are blends of slab and mantle materials. This conclusion is similar to that of Straub *et al.* (2008), with the only difference being that now P and Nb are also identified as partially recycled elements. The model emphasizes the importance of the slab flux relative to the mantle contributions, and attributes much of the arc-typical major element

Table 5: Parameters for melting curves in Ti_{88}–P_{88} space in Fig. 25

	P	Ti
Mantle wedge[1]	95 ppm	1300 ppm
Mineral/melt partition coefficients[2]		
Olivine	0·1	0·013
Orthopyroxene	0·03	0·1
Clinopyroxene	0·05	0·27

	Peridotite source	Pyroxenite source			
	Curves 1–4	Curve 1	Curve 2	Curve 3	Curve 4
Phase proportion in mantle source (%)					
Olivine	59	59	40	30	10
Orthopyroxene	21	21	40	55	75
Clinopyroxene	20	20	20	15	15

[1]Corresponds to abundances of primitive mantle from Sun & McDonough (1989)
[2]Partition coefficients from Brunet & Chazot (2001) and Adam & Green (2006).

signatures to slab–mantle mixing, and not to crustal differentiation. It is entirely possible, however, that other 'OIB-type' arc magmas of the MVB may have weaker slab signals than the Texcal Flow and V. Chichinautzin magmas, and hence provide more information about mantle composition (Gómez-Tuena *et al.*, 2011).

CONCLUSIONS

The major results of this study can be summarized as follows.

(1) Zoned monogenetic arc volcanoes are an excellent means of deciphering the processes of magmatic differentiation in arc magmas.
(2) Texcal Flow and V. Chichinautzin magmas are hybrids of initial basaltic to dacitic mantle-derived melts from pyroxenite lithologies that are moderately modified by processing in the overlying crust.
(3) The temporal increase in silica content in Texcal Flow and V. Chichinautzin magmas does not reflect fractional crystallization or crustal contamination, but is ultimately a consequence of the addition of silicic slab components to the mantle wedge.
(4) The major element contents of Texcal Flow and V. Chichinautzin lavas are blends of elements from the subarc mantle (Ti, Fe, Mg, Ca) and of elements contributed from the subducted slab (Na, K, P). Si, and possibly Al, is contributed in significant amounts from both of these reservoirs.
(5) The mantle beneath Texcal Flow and V. Chichinautzin is at least as enriched as primitive mantle, but not as enriched as the mantle sources of the Mexican Basin and Range basalts.

ACKNOWLEDGEMENTS

Rick Conrey, Diane Johnson, Beth Goldoff, Steve Goldstein, Wen-Yu Hsu, Charles Mandeville, Ofélia Pérez-Arvizu, Dave Walker and Susan Woods are thanked for laboratory support. Joshua Brown and Amy Knorpp helped with sample preparation, and Jason Jweda, Laura Mori, Peri Sasnett and Jill van Tongeren assisted in the field. We are grateful to Dawnika Blatter, David Peate and an anonymous reviewer for constructive and insightful reviews.

FUNDING

This study was financially supported by the US National Science Foundation (grant EAR-07-38707 to S.M.S.) and the National Science Council of Taiwan (grants 96-2811-M-001-023 and 98-2811-M-001-052 to G.F.Z.).

SUPPLEMENTARY DATA

Supplementary data for this paper are available at *Journal of Petrology* online.

REFERENCES

Adam, J. & Green, T. (2006). Trace element partitioning between mica- and amphibole-bearing garnet lherzolite and hydrous basanitic melt: l. Experimental results and the investigation of controls on partitioning behaviour. *Contributions to Mineralogy and Petrology* **152**, 1–17, doi:10.1007/s00410-010-0570-7.

Allègre, C. J., Staudacher, T. & Sarda, P. (1986–1987). Rare gas systematics: formation of the atmosphere evolution and structure of the Earth's mantle. *Earth and Planetary Science Letters* **81**, 127–150.

Annen, C., Blundy, J. D. & Sparks, R. S. J. (2006). The genesis of intermediate and silicic magmas in deep crustal hot zones. *Journal of Petrology* **47**, 505–539, doi:10.1093/petrology/egi084.

Baker, M. B., Grove, T. L. & Price, R. (1994). Primitive basalts and andesites from the Mt. Shasta region, N. California: products of varying melt fraction and water content. *Contributions to Mineralogy and Petrology* **118**, 111–129.

Ballentine, C. J. & Burnard, P. G. (2002). Production, release and transport of noble gases in the continental crust. In: Porcelli, D. P., Ballentine, C. J. & Wieler, R. (eds) *Noble Gases. Mineralogical Society of America and Geochemical Society, Reviews in Mineralogy and Geochemistry* **47**, 481–538.

Beard, J. S. & Lofgren, G. E. (1991). Dehydration melting and water-saturated melting of basaltic and andesitic greenstones and amphibolites at l, 3 and 6·9 kbar. *Journal of Petrology* **32**, 365–401.

Beattie, P., Ford, C. & Russell, D. (1991). Partition coefficients for olivine–melt and orthopyroxene–melt systems. *Contributions to Mineralogy and Petrology* **109**, 212–224.

Blatter, D. L. & Carmichael, I. S. E. (1998). Plagioclase-free andesites from Zitacuaro (Michoacan), Mexico: petrology and experimental constraints. *Contributions to Mineralogy and Petrology* **132**, 121–138.

Blatter, D. L., Carmichael, I. S. E., Deino, A. L. & Renne, P. R. (2001). Neogene volcanism at the front of the central Mexican volcanic belt: basaltic andesites to dacites, with contemporaneous shoshonites and high-TiO_2 lavas. *Geological Society of America Bulletin* **113**, 1324–1342.

Blatter, D. L., Farmer, G. L. & Carmichael, I. S. E. (2007). A north–south transect across the Central Mexican Volcanic Belt at c. 100°N: Spatial distribution, petrological, geochemical and isotopic characteristics of Quaternary volcanism. *Journal of Petrology* **48**, 901–950, doi:10.1093/petrology/egm006.

Brunet, F. & Chazot, G. (2001). Partitioning of phosphorus between olivine, clinopyroxene and silicate glass in a spinel lherzolite xenolith from Yemen. *Chemical Geology* **176**, 51–72.

Carmichael, I. S. E. (2002). The andesite aqueduct: perspectives on the evolution of intermediate magmatism in west–central (105–99°W) Mexico. *Contributions to Mineralogy and Petrology* **143**, 641–663.

Cervantes, P. & Wallace, P. J. (2003*a*). The role of H_2O in subduction zone magmatism: New insights from melt inclusions in high-Mg basalts from central Mexico. *Geology* **31**, 235–238.

Cervantes, P. & Wallace, P. J. (2003*b*). Magma degassing and basaltic eruption styles: a case study of V2000 year BP Xitle volcano in central Mexico. *J Volcanol Geotherm Res* **120**, 249–270.

Davidson, J., Turner, S., Handley, H., Macpherson, C. & Dosseto, A. (2007). Amphibole 'sponge' in arc crust? *Geology* **35**, 787–790, doi:10.1130/G23637A.1.

Davis, F. A., Hirschmann, M. M. & Humayun, M. (2011). The composition of the incipient partial melt of garnet peridotite at 3 GPa and the origin of OIB. *Earth and Planetary Science Letters* **308**, 380–390, doi:10.1016/j.epsl.2011.06.008.

Defant, M. & Drummond, M. (1990). Derivation of some modern arc magmas by melting of young subducted lithosphere. *Nature* **347**, 662–665.

Donnelly, K., Goldstein, S. L., Langmuir, C. H. & Spiegelman, M. (2004). Origin of enriched ocean ridge basalt and implications for mantle dynamics. *Earth and Planetary Science Letters* **226**, 347–366.

Eichelberger, J. C. (1978). Andesitic volcanism and crustal evolution. *Nature* **275**, 21–27.

Farley, K. A. & Neroda, E. (1998). Noble gases in the Earth's mantle. *Annual Review of Earth and Planetary Sciences* **26**, 189–218.

Ferrari, L., Orozco-Esquivel, M. T., Manea, V. C. & Manea, M. (2011). The dynamic history of the Trans-Mexican Volcanic Belt and the Mexico subduction zone. *Tectonophysics*, 522–523, 122–149, doi:10.1016/j.tecto.2011.09.018.

Freundt, A. & Schmincke, H. U. (1995). Petrogenesis of rhyolite–trachyte–basalt composite ignimbrite Pl, Gran Canaria, Canary Island. *Journal of Geophysical Research* **100**, 455–474.

GeoROC (2011). *Geochemistry of Rocks of the Oceans and Continents*, World Wide Web Address: http://georoc.mpch-mainz.gwdg.de/georoc/.

Gill, J. (1981). *Orogenic Andesites and Plate Tectonics*. Berlin: Springer.

Gómez-Tuena, A., LaGatta, A., Langmuir, C. H., Goldstein, S. L., Ortega-Gutiérrez, F. & Carrasco-Nunez, G. (2003). Temporal control of subduction magmatism in the eastern Trans-Mexican Volcanic Belt: Mantle sources, slab contributions, and crustal contamination. *Geochemistry, Geophysics, Geosystems* **8**, 8913, doi:10.1029/2003GC000524.

Gómez-Tuena, A., Langmuir, C. H., Goldstein, S. L., Straub, S. M. & Ortega-Gutierrez, F. (2007*a*). Geochemical evidence for slab melting in the Trans-Mexican Volcanic Belt. *Journal of Petrology* **48**, 537–562, doi:10.1093/petrology/egl071.

Gómez-Tuena, A., Orozco-Esquivel, M. T. & Ferrari, L. (2007*b*). Igneous petrogenesis of the Trans-Mexican Volcanic Belt. In: Alaniz-Álvarez, S. A. & Nieto-Samaniego, Á. F. (eds) *Geology of México: Celebrating the Centenary of the Geological Society of México. Geological Society of America, Special Papers* **422**, 129–181.

Gómez-Tuena, A., Laura Mori, L., Goldstein, S. L. & Perez-Arvizu, O. (2011). Magmatic diversity of western Mexico as a function of metamorphic transformations in the subducted oceanic plate. *Geochimica et Cosmochimica Acta* **75**, 213–241, doi:10.1016/j.gca.2010.09.029.

Green, T. H. & Watson, E. B. (1982). Crystallization of apatite in natural magmas under high pressure, hydrous conditions, with particular reference to orogenic rock series. *Contributions to Mineralogy and Petrology* **79**, 96–105.

Gurenko, A. A., Hansteen, T. H. & Schmincke, H. U. (1996). Evolution of parental magmas of Miocene shield basalts of Gran Canaria (Canary Islands): constraints from crystal, melt and fluid inclusions. *Contributions to Mineralogy and Petrology* **124**, 422–435.

Hall, P. S. & Kincaid, C. (2001). Diapiric flow at subduction zones: a recipe for rapid transport. *Science* **292**, 2472–2475.

Hermann, J., Spandler, C., Hack, A. & Korsakov, A. V. (2006). Aqueous fluids and hydrous melts in high-pressure and ultra-high pressure rocks: Implications for element transfer in subduction zones. *Lithos* **92**, 399–417, doi:10.1016/j.lithos.2006.03.055.

Herzberg, C. (2011). Identification of source lithology in the Hawaiian and Canary Islands: implications for origins. *Journal of Petrology* **52**, 113–146, doi:10.1093/petrology/egq075.

Hildreth, W. & Moorbath, S. (1988). Crustal contributions to arc magmatism in the Andes of Central Chile. *Contributions to Mineralogy and Petrology* **98**, 455–489.

Hirose, K. (1997). Melting experiments on lherzolite KLB-1 under hydrous conditions and generation of high-magnesian andesitic melts. *Geology* **25**, 42–44.

Irvine, T. N. & Baragar, W. R. A. (1971). A guide to the chemical classification of the common volcanic rocks. *Canadian Journal of Earth Sciences* **8**, 523–548.

Ishimaru, S. & Arai, S. (2008). Nickel enrichment in mantle olivine beneath a volcanic front. *Contributions to Mineralogy and Petrology* **156**, 119–131, doi:10.1007/s00410-007-0277-6.

Johnson, E. R., Wallace, P. J., Delgado-Granados, H., Manea, V. C., Kent, A. J. R., Bindeman, I. N. & Donegan, C. S. (2009). Subduction-related volatile recycling and magma generation beneath central Mexico: insights from melt inclusions, oxygen isotopes and geodynamic models. *Journal of Petrology* **50**, 1729–1764, doi:10.1093/petrology/egp051.

Johnson, M. C. & Plank, T. (1999). Dehydration and melting experiments constrain the fate of subducted sediment. *Geochemistry, Geophysics, Geosystems* **1**, 1999GC000014.

Kay, R. W. (1978). Aleutian magnesian andesites: melts from subducted Pacific Ocean crust. *Journal of Volcanology and Geothermal Research* **4**, 117–132.

Kelemen, P. B. (1995). Genesis of high Mg# andesites and the continental crust. *Contributions to Mineralogy and Petrology* **120**, 1–19.

Kelemen, P. B., Yogodzinksi, G. & Scholl, D. W. (2003). Along-strike variation in the Aleutian island arc: Genesis of high-mg# andesite and implication for the continental crust. In: Eiler, J. (ed.) *Inside the Subduction Factory. American Geophysical Union, Geophysical Monograph* **138**, 223–276.

Kelemen, P. B., Hanghoi, K. & Greene, A. R.One view of the geochemistry of subduction-related magmatic arcs, with an emphasis on primitive andesite and lower crust. In: Rudnick, R. L. (ed.)

The Crust. Treatise on Geochemistry, Vol. 3. Oxford: Elsevier-Pergamon, pp. 593–659.

Kent, A. J. R., Darr, C., Koleszar, A. M., Salisbury, M. J. & Cooper, K. M. (2010). Preferential eruption of andesitic magmas through recharge filtering. *Nature Geoscience* **3**, 631–636, doi:10.1038/ngeo924.

Kessel, R., Schmidt, M. W., Ulmer, P. & Pettke, T. (2005). Trace element signature of subduction-zone fluids, melts and supercritical liquids at 120–180 km depth. *Nature* **437**, 724–727, doi:10.1038/nature03971.

Kessel, R., Ulmer, P., Schmidt, M. W. & Pettke, T. (2008). *Experimental constraints on trace element partitioning during dehydration and melting of K-free MORB at 4–6 GPa and 700–1200°C*, EOS Transactions American Geophysical Union 89(53), Fall Meeting Supplement, Abstract V31F-01.

Kim, Y., Clayton, R. W. & Jackson, J. M. (2010). Geometry and seismic properties of the subducting Cocos plate in central Mexico. *Journal of Geophysical Research* **115**, doi:10.1029/2009JB006942.

Klemme, S., Prowatke, S., Hametner, K. & Guenther, D. (2005). Partitioning of trace elements between rutile and silicate melts: Implications for subduction zones. *Geochimica et Cosmochimica Acta* **69**, 2361–2371, doi:10.1016/j.gca.2004.11.015.

Klimm, K., Blundy, J. D. & Green, T. H. (2008). Trace element partitioning and accessory phase saturation during H_2O-saturated melting of basalt with implications for subduction zone chemical fluxes. *Journal of Petrology* **49**, 523–553, doi:10.1093/petrology/egn001.

Kogiso, T., Hirschmann, M. & Pertermann, M. (2004). High-pressure partial melting of mafic lithologies in the mantle. *Journal of Petrology* **45**, 2407–2422, doi:10.1093/petrology/egh057.

Kuno, H. (1966). Lateral variation of basalt magma typ across continental margins and island arcs. *Bulletin of Volcanology* **29**, 195–222.

LaGatta, A. B. (2003). *Arc Magma Genesis in the Eastern Mexican Volcanic Belt*. New York: Columbia University, 329 p.

Langmuir, C. H. (1989). Geochemical consequences of *in-situ* crystallisation. *Nature* **340**, 199–205.

Langmuir, C. H., Klein, E. M. & Plank, T. (1992). Petrological systematics of mid-ocean ridge basalts: constraints on melt generation beneath ocean ridges. In: Morgan, J. P., Blackman, D. K. & Sinton, J. M. (eds) *Mantle Flow and Melt Generation at Mid-Ocean Ridges. American Geophysical Union, Geophysical Monograph* **71**, 183–280.

Lawlor, P. J., Ortega-Gutierrez, F., Cameron, K. L., Ochoa-Camarillo, H., Lopez, R. & Sampson, D. E. (1999). U–Pb geochronology, geochemistry, and provenance of the Grenvillian Huiznopala Gneiss of Eastern Mexico. *Precambrian Research* **94**, 73–99.

Leeman, W. P. (1983). The influence of crustal structure on compositions of subduction-related magmas. *Journal of Volcanology and Geothermal Research* **18**, 561–588.

Luhr, J. F. (1997). Extensional tectonics and the diverse primitive volcanic rocks in the western Mexican Volcanic Belt. *Canadian Mineralogist* **35**, 473–500.

Luhr, J. F. & Carmichael, I. S. E. (1985). Jorullo Volcano, Michoacán, Mexico (1759–1774): The earliest stages of fractionation in calc-alkaline magmas. *Contributions to Mineralogy and Petrology* **90**, 142–161.

Luhr, J. F., James, F. A., Carmichael, I. S. E., Nelson, S. A. & Hasenaka, T. (1989). Primitive calc-alkaline and alkaline rock types from the Western Mexican Volcanic Belt. *Journal of Geophysical Research* **94**, 4515–4530.

Luhr, J. F., Aranda-Gomez, J. J. & Housh, T. (1995*a*). San Quintin Volcanic Field, Baja California Norte, Mexico: Geology, petrology, and geochemistry. *Journal of Geophysical Research* **100**, 10353–10380.

Luhr, J. F., Pier, J. G., Aranda-Gomez, J. J. & Posedek, F. A. (1995*b*). Crustal contamination in early Basin-and-Range hawaiites of the Los Encinos Volcanic Field, central Mexico. *Contributions to Mineralogy and Petrology* **118**, 321–339.

Marquez, A., Verma, S. P., Anguita, F., Oyarzin, R. & Brandle, J. L. (1999). Tectonics and volcanism of Sierra Chichinautzin: extension at the front of the Central Trans-Mexican Volcanic Belt. *Journal of Volcanology and Geothermal Research* **93**, 125–150.

Martelli, M., Nuccio, P. M., Stuart, F. M., Di Liberto, V. & Ellam, R. M. (2008). Constraints on mantle source and interactions from He–Sr isotope variation in Italian Plio-Quaternary volcanism. *Geochemistry, Geophysics, Geosystems* **9**, Q02001, doi:10.1029/2007GC001730.

Martinez-Serrano, R. G., Schaaf, P., Solids-Pichardo, G., Hernandez-Bernal, M. S., Hernandez-Trevino, T., Morales-Contreras, J. J. & Macias, J. L. (2004). Sr, Nd and Pb isotope and geochemical data from the Quaternary Nevado the Toluca volcano, a source of recent adakite magmatism, and the Tenango Volcanic Field. *Journal of Volcanology and Geothermal Research* **138**, 77–110.

Matzen, A. K., Baker, M. B., Beckett, J. R. & Stolper, E. M. (2012). Ni partitioning between olivine and high-MgO silicate melts: Implications for Ni contents of forsteritic phenocrysts in basalts. *22nd V.M. Goldschmidt Conference*, 24–29 June 2012, Montreal, Canada.

Maurel, C. & Maurel, P. (1982). Etude expérimentale de l'équilibre Fe^{2+}–Fe^{3+} dans les spinelles chromifères et les liquides silicates basiques, à 1 atm. *Comptes Rendus de l'Académie des Sciences, Série II* **295**, 209–212.

McBirney, A., Taylor, H. & Armstrong, R. (1987). Paricutin re-examined: a classic example of crustal assimilation in a calc-alkaline magma. *Contributions to Mineralogy and Petrology* **95**, 4–20.

McDonough, W. F. & Sun, S. S. (1995). The composition of the Earth. *Chemical Geology* **120**, 223–253.

Moore, G. & Carmichael, I. S. E. (1998). The hydrous phase equilibria (to 3 kbar) of an andesite and basaltic andesite from western Mexico: constraints on water content and conditions of phenocryst growth. *Contributions to Mineralogy and Petrology* **130**, 304–319.

Moreira, M. & Sarda, P. (2000). Noble gas constraints on degassing process. *Earth and Planetary Science Letters* **176**, 375–386.

Niu, Y. & Batiza, R. (1997). Trace element evidence from seamounts for recycled oceanic crust in the Eastern Pacific mantle. *Earth and Planetary Science Letters* **148**, 471–483.

Nixon, G. T. (1988*a*). Petrology of the younger andesites and dacites of Iztaccihuatl Volcano, Mexico: I. Disequilibrium phenocrysts assemblages as indicators of magma chamber processes. *Journal of Petrology* **29**, 213–264.

Nixon, G. T. (1988*b*). Petrology of the younger andesites and dacites of Iztaccihuatl Volcano, Mexico: II. Chemical stratigraphy, magma mixing, and the composition of basaltic magma influx. *Journal of Petrology* **29**, 265–303.

O'Nions, R. K. & Oxburgh, E. R. (1988). Helium, volatile fluxes and the development of continental crust. *Earth and Planetary Science Letters* **90**, 331–347.

Ortega-Gutiérrez, F., Elías-Herrera, M. & Dávalos-Elizondo, M. G. (2008). On the nature and role of the lower crust in the volcanic front of the Trans-Mexican Volcanic Belt and its fore-arc region, southern and central Mexico. *Revista Mexicana de Ciencias Geológicas* **25**, 346–364.

Pardo, M. & Suarez, G. (1995). Shape of the subducted Rivera and Cocos plate in southern Mexico: seismic and tectonic implications. *Journal of Geophysical Research* **100**, 12357–12373.

Perez-Campos, X., Kim, Y. H., Husker, A., Davis, P. M., Clayton, R. W., Iglesias, A., Pacheco, J. F., Singh, S. K., Manea, V. C. &

Gurnis, M. (2008). Horizontal subduction and truncation of the Cocos Plate beneath central Mexico. *Geophysical Research Letters* **35**, 18303, doi:10.1029/2008GL035127.

PetDB (2011). *Information System for Geochemical Data of Igneous and Metamorphic Rocks from the Ocean Floor*, World Wide Web Address: http://www.petdb.org/petdbWeb/index.jsp.

Plank, T. & Langmuir, C. H. (1988). An evaluation of the global variations in the major element chemistry of arc basalts. *Earth and Planetary Science Letters* **90**, 349–370.

Plank, T. & Langmuir, C. H. (1993). Tracing trace elements from sediment input to volcanic output at subduction zones. *Nature* **362**, 739–743.

Rapp, R. P. & Watson, E. B. (1995). Dehydration melting of metabasalt at 8–32 kbar: Implications for continental growth and crust–mantle recycling. *Journal of Petrology* **36**, 891–931.

Rapp, R. P., Shimizu, N., Norman, M. D. & Applegate, G. S. (1999). Reaction between slab-derived melts and peridotite in the mantle wedge: experimental constraints at 3·8 GPa. *Chemical Geology* **160**, 335–356.

Reiners, P. W. (2002). Temporal–compositional trends in intraplate basalt eruptions: Implications for mantle heterogeneity and melting processes. *Geochemistry, Geophysics, Geosystems* **3**, doi:10.1029/2001GC000250.

Reubi, O. & Blundy, J. (2009). A dearth of intermediate melts at subduction zone volcanoes and the petrogenesis of arc andesites. *Nature* **461**, 1269–1273, doi:10.1038/nature08510.

Roberge, J., Delgado-Granados, H. & Wallace, P. J. (2009). Mafic magma recharge supplies high CO_2 and SO_2 gas fluxes from Popocatépetl volcano, Mexico. *Geology* **37**, 107–110, doi:10.1130/G25242A.1.

Roberts, S. J. & Ruiz, J. (1989). Geochemistry of exposed granulite facies terrains and lower crustal xenoliths in Mexico. *Journal of Geophysical Research* **94**, 7961–7974.

Robin, C., Eissen, J. P. & Monzier, M. (1994). Ignimbrites of basaltic andesite and andesite compositions from Tanna, New Hebrides Arc. *Bulletin of Volcanology* **56**, 10–22.

Roeder, P. E. & Emslie, R. F. (1970). Olivine–liquid equilibrium. *Contributions to Mineralogy and Petrology* **29**, 275–289.

Rudnick, R. & Gao, S. (2002). Composition of the continental crust. In: Rudnick, R. L. (ed.) *The Crust. Treatise on Geochemistry*, . Oxford: Elsevier–Pergamon **Vol. 3**1–64.

Ruiz, J., Patchett, J. & Arculus, R. J. (1988). Nd–Sr isotope composition of lower crustal xenoliths—Evidence for the origin of mid-Tertiary felsic volcanics in Mexico. *Contributions to Mineralogy and Petrology* **99**, 36–43.

Sarda, P. & Graham, D. W. (1990). Mid-ocean ridge popping rocks and outgassing processes at ridge crests. *Earth and Planetary Science Letters* **97**, 268–289.

Savov, I. P., Ryan, J. G., D'Antonio, M., Kelley, K. & Mattie, P. (2005). Geochemistry of serpentinized peridotites from the Mariana Forearc Conical Seamount, ODP Leg 125: Implications for the elemental recycling in subduction zones. *Geochemistry, Geophysics, Geosystems* **6**, doi:10.1029/2004GC000777.

Schaaf, P., Heinrich, W. & Besch, T. (1994). Composition and Sm–Nd isotopic data of the lower crust beneath San Luis Potosi, central Mexico: evidence from a granulite-facies xenolith suite. *Chemical Geology* **118**, 63–84.

Schaaf, P., Stimac, J., Siebe, C. & Macias, J. L. (2005). Geochemical evidence for mantle origin and crustal processes in volcanic rocks from Popocatepetl and surrounding monogenetic volcanoes, central Mexico. *Journal of Petrology* **46**, 1243–1282.

Siebe, C., Rodriguez-Lara, V., Schaaf, P. & Abrams, M. (2004*a*). Geochemistry, Sr–Nd isotope composition, and tectonic setting of Holocene Pelado, Guespalapa and Chichinautzin scoria cones, south of Mexico City. *Journal of Volcanology and Geothermal Research* **130**, 197–226.

Siebe, C., Rodriguez-Lara, V., Schaaf, P. & Abrams, M. (2004*b*). Radiocarbon ages of Holocene Pelado, Guespalapa, and Chichinautzin scoria cones, south of Mexico City: implications for archeology and future hazards. *Bulletin of Volcanology* **66**, 203–225, doi:10.1007/s00445-00003-00304-z.

Skora, S. & Blundy, J. (2010). High-pressure hydrous phase relations of radiolarian clay and implications for the involvement of subducted sediment in arc magmatism. *Journal of Petrology* **51**, 2211–2243, doi:10.1093/petrology/egq054.

Sobolev, A. V., Hofmann, A. W., Sobolev, V. S. & Nikogosian, I. K. (2005). An olivine-free mantle source of Hawaiian shield basalts. *Nature* **434**, 590–597.

Stolz, A. J., Jochum, K. P., Spettel, B. & Hofmann, A. W. (1996). Fluid- and melt-related enrichment in the subarc mantle: Evidence from Nb/Ta variations in island-arc basalts. *Geology* **24**, 587–590.

Straub, S. M. & Martin-Del Pozzo, A. L. (2001). The significance of phenocryst diversity in tephra from recent eruptions at Popocatepetl volcano (Central Mexico). *Contributions to Mineralogy and Petrology* **140**, 487–510.

Straub, S. M. & Zellmer, G. F. (2012). Volcanic arcs as archives of plate tectonic change. *Gondwana Research* **21**, 495–516, doi:10.1016/j.gr.2011.10.006.

Straub, S. M., LaGatta, A. B., Martin-Del Pozzo, A. L. & Langmuir, C. H. (2008). Evidence from high Ni olivines for a hybridized peridotite/pyroxenite source for orogenic andesites from the central Mexican Volcanic Belt. *Geochemistry, Geophysics, Geosystems* **9**, Q03007, doi:10.1029/2007GC001583.

Straub, S. M., Gómez-Tuena, A., Stuart, F. M., Zellmer, G. F., Espinasa-Perena, R., Cai, M. Y. & Iizuka, Y. (2011*a*). Formation of hybrid arc andesites beneath thick continental crust. *Earth and Planetary Science Letters* **303**, 337–347, doi:10.1016/j.epsl.2011.01.013.

Straub, S. M., Zellmer, G. F., Gómez-Tuena, A., Stuart, F. M., Espinasa-Perena, R. & Cai, Y. (2011*b*). Mantle origin of silicic calc-alkaline basalts to andesites in the Central Mexican Volcanic Belt. Eos Trans. American Geophysical Union 92, Fall Meeting Supplement, Abstract V32C-04.

Streck, M. J., Leeman, W. P. & Chesley, J. (2007). High-magnesian andesite from Mount Shasta: a product of magma mixing and contamination, not a primitive mantle melt. *Geology* **35**, 351–354, doi:10.1130/G23286A.1.

Stuart, F. M., Ellam, R. M., Harrop, P. J., Fitton, J. G. & Bell, B. R. (2000). Constraints on mantle plumes from the helium isotopic composition of basalts from the British Tertiary Igneous Province. *Earth and Planetary Science Letters* **177**, 273–285.

Sun, S. S. & McDonough, W. F. (1989). Chemical and isotopic systematics of oceanic basalts: implications for mantle composition and processes. In: Saunders, A. D. & Norry, M. J. (eds) *Magmatism in the Ocean Basins. Geological Society, London, Special Publications* **42**, 313–345.

Tamura, Y. & Tatsumi, Y. (2002). Remelting of an andesitic crust as a possible origin for rhyolitic magma in oceanic arcs: an example from the Izu–Bonin Arc. *Journal of Petrology* **43**, 1029–1047.

Tatsumi, Y. & Eggins, E. (1995). *Subduction Zone Magmatism*. Cambridge, MA: Blackwell Science.

Verma, S. P. (1999). Geochemistry of evolved magmas and their relationship to subduction-unrelated mafic volcanism at the volcanic front of the central Mexican Volcanic Belts. *Journal of Volcanology and Geothermal Research* **93**, 151–171.

Wallace, P. J. & Carmichael, I. S. E. (1999). Quaternary volcanism near the Valley of Mexico: implications for subduction zone magmatism and the effects of crustal thickness variations on primitive

magma compositions. *Contributions to Mineralogy and Petrology* **135**, 291–314.

Weaver, S. L., Wallace, P. J. & Johnston, D. A. (2011). A comparative study of continental vs intraoceanic arc mantle melting: Experimentally determined phase relations of hydrous primitive melts. *Earth and Planetary Science Letters* **308**, 97–106, doi:10.1016/j.epsl.2011.05.040.

Weber, R. M., Wallace, P. J. & Johnston, A. D. (2011). Experimental insights into the formation of high-Mg basaltic andesites in the trans-Mexican volcanic belt. *Contributions to Mineralogy and Petrology online*, doi:10.1007/s00410-011-0701-9.

Wilcox, R. E. (1954). Petrology of Paricutin Volcano, Mexico. *US Geological Survey Bulletin* **965-C**, 281–354.

Workman, R. K. & Hart, S. R. (2005). Major and trace element composition of the depleted MORB mantle (DMM). *Earth and Planetary Science Letters* **231**, 53–72.

Yogodzinksi, G., Volynets, O. N., Koloskov, A. V., Seliverstov, N. I. & Matvenko, V. V. (1994). Magnesian andesites and the subduction component in a strongly calc-alkaline series at Piip Volcano, far western Aleutians. *Journal of Petrology* **35**, 163–204.

Yogodzinski, G. M., Kay, R. W., Volynets, O. N., Koloskov, A. V. & Kay, S. M. (1995). Magnesian andesite in the western Aleutian Komandorsky region: Implications for slab melting and processes in the mantle wedge. *Geological Society of America Bulletin* **107**, 505–519.